

## General Disclaimer

### One or more of the Following Statements may affect this Document

- This document has been reproduced from the best copy furnished by the organizational source. It is being released in the interest of making available as much information as possible.
- This document may contain data, which exceeds the sheet parameters. It was furnished in this condition by the organizational source and is the best copy available.
- This document may contain tone-on-tone or color graphs, charts and/or pictures, which have been reproduced in black and white.
- This document is paginated as submitted by the original source.
- Portions of this document are not fully legible due to the historical nature of some of the material. However, it is the best reproduction available from the original submission.



DEVELOPMENT OF A BREADBOARD MULTIELEMENT STAR DETECTOR

By A. Asam - W. Hell - R. Haas

December 1968

Prepared under Contract No. NAS 5-10340 by

THE MARQUARDT CORPORATION

Van Nuys, California

for

NASA

GODDARD SPACE FLIGHT CENTER

GREENBELT, MARYLAND

## ABSTRACT

The objective of this contract was to adapt Marquardt's sensing techniques to star pattern detection from a spinning spacecraft. A tradeoff design study indicates that a multielement detector strip employing a unique combination of a thin film photoconductor for optical sensing and a highly non-linear dielectric material, i.e., a ferroelectric, for signal integration can produce usable signals from low level photon irradiance produced by stars such as Alpheratz. An investigation of sensor strip readout methods proved that a commutator for sampling the elemental signals can be realized by thin film materials which would be compatible with the photoconductor/ferroelectric material combination. Thin film switching elements (TFT) based on CdS-Se materials were produced exhibiting a transconductance of 2000 microamperes per volt which is satisfactory for multiplexing the detector strip. Experiments with a multielement, thin film detector strip have demonstrated that elemental signal integration and signal storage is feasible that would enhance the star pattern detection capabilities.



TABLE OF CONTENTS

	<u>Page No.</u>
ABSTRACT	
TABLE OF CONTENTS	
LIST OF ILLUSTRATIONS	
I. INTRODUCTION	1
II. REQUIREMENTS	2
III. SYSTEM DESIGN CONSIDERATIONS	3
IV. READOUT TECHNIQUES	9
A. Theory	9
B. Experiments	14
V. THIN FILM DETECTOR STRIP EVALUATION	20
VI. THIN FILM MATERIAL DEVELOPMENT	25
VII. CONCLUSIONS AND RECOMMENDATIONS	36
APPENDIX I - STAR DETECTOR CONCEPT	37
APPENDIX II - STAR BRIGHTNESS COMPUTATION	42

LIST OF ILLUSTRATIONS

<u>Figure No.</u>		<u>Page No.</u>
1.	Photoconductor Configurations	5
2.	TFT Structure and Dimensions	10
3.	Control Mechanism and Characteristics	11
4.	Discrete Element Commutator	15
5.	TFT Equivalent Circuit	16
6.	Commutator Electrode Configuration	17
7.	Typical Component Pattern of a 50 Line Commutator	18
8.	Detector Strip Geometry	21
9.	Star Pattern Simulator	22
10.	Detector Strip Integration	24
11.	Photomicrograph of Surface of Deposited CdS Film	26
12.	Photomicrograph of Surface of Deposited CdS Film	27
13.	Photomicrograph of Surface of Deposited CdS Film	29
14.	Photomicrograph of Surface of Deposited CdS Film	30
15.	Photomicrograph of Surface of Deposited CdS Film	32
16.	Photomicrograph of Surface of Deposited CdS Film	33
17.	Photomicrograph of Surface of Deposited CdS Film	34
18.	Detector Element	38
19.	Multielement Detector for Star Pattern Recognition System	39
20.	Multiple Exposure for Low Light Level Integration	41
21.	Correction from Radiometric to Photon Magnitude	46

I. INTRODUCTION

This report describes the work performed under Contract NAS 5-10340 for the period March 1967 to September 1967. The primary objective was to investigate the aspects of star detection from a spinning spacecraft by signal integration with a thin film detector strip and to evaluate TFT commutation in readout. The nucleus of the concept for this system is a unique combination of thin film photo-sensitive and high dielectric materials for sensing, integrating, and permanently storing low as well as high light level signals until readout.

The work reported covers a design study to examine the compatibility of the proposed system with light levels from typical stars, the fabrication and test of a thin film detector strip, and the investigation of the use of thin film transistors for commutation purposes.

## II. REQUIREMENTS

The recognition of star patterns for the purpose of attitude determination of spin stabilized spaceborne vehicles relies upon the optical acquisition of a star field focussed onto a high resolution photosensitive mosaic and comparison with a reference star pattern. The generally accepted characteristics for such a spaceborne system include maximum gain in detection in conjunction with a low threshold sensing capability, and a low signal to noise figure of merit. The need for a high angular resolution makes a short exposure time in sensing very desirable. Further incidental but necessary requirements include low power, low weight, and a minimum volume. The Marquardt concept for a thin film star detection system which can meet these requirements is described in Appendix I. (This system is a line array of small elemental areas which permit repeated exposure for the integration of weak signals and a commutated readout).

The sensing of individual stars in a given pattern requires a detection operation which must cover many orders of magnitude. It is possible to detect weak signals from stars for pattern recognition purposes with an extremely sensitive quantum detector. However, the requirements for the detector can be less stringent when an integrating function can be incorporated into the system. The use of this integration feature permits a signal to noise enhancement that is not possible with other detection schemes.

The system design considerations, readout techniques, and the thin film material development are discussed below.

### III. SYSTEM DESIGN CONSIDERATIONS

In order to achieve maximum gain, the lowest possible threshold in sensing, and a high angular resolution, it is necessary to consider the relation of the detection phenomena to the mode of operation and geometry of the detection elements. These system design considerations are presented in the following sections.

The geometry and mode of operation of the photoconductive elements in the detector strip are to be influenced by

the need for maximum gain as related to specific properties of processed cadmium sulfide material

the consideration that a high resistance photoconductor is desirable

the goal of maximum resolution independent of the optical system but related to the necessary exposure time during system operation

If we examine the commonly used expression for gain in a bulk detector such as a photoconductor,

$$G = \frac{\tau}{T_T} = \frac{\tau u V}{d^2}$$

where  $\tau$  = the lifetime of a free carrier in seconds

$u$  = the mobility in  $\text{cm}^2 \text{ volt}^{-1} \text{ sec}^{-1}$   
a material characteristic

$V$  = the applied voltage in volts

$d$  = the electrode gap in cm

$T_T$  = the electrode transit time in seconds

it can be seen that the gain can be increased by decreasing the transit time,  $T_T$ . Since the mobility,  $u$ , is determined by the material processing,  $T_T$  can be decreased by increasing the applied voltage or by decreasing the electrode gap. The maximum operating voltage, if impact ionization is neglected, is limited by dielectric breakdown of the material which occurs at approximately  $10^5$  volts  $\text{cm}^{-1}$  for cadmium

sulfide, CdS. The minimum electrode spacing,  $d$ , will depend on whether the detector is operated in the surface or coplanar electrode mode or the volume mode. In the surface mode, conventional masking techniques will permit a minimum gap of approximately 0.5 mil. In the volume mode, the thickness of deposition calls for an electrode gap of approximately 1 micron. A comparison of the factor,  $\frac{V}{d^2}$ , for the two configurations provides a rough measure of the difference in gain that can be realized.

In the surface mode, the maximum operating voltage is equal to the product of the breakdown field and the gap, or

$$10^5 \text{ volts cm}^{-1} \times 0.5 \times 2.5 \times 10^{-3} \text{ cm} = 125 \text{ volts}$$

therefore,

$$\frac{V}{d^2} = \frac{125}{(1.25 \times 10^{-3})^2} = 0.8 \times 10^8 \text{ volts cm}^{-2}$$

For the volume case, the maximum operating voltage is

$$10^5 \text{ volts cm}^{-1} \times 10^{-4} \text{ cm} = 10 \text{ volts}$$

and,

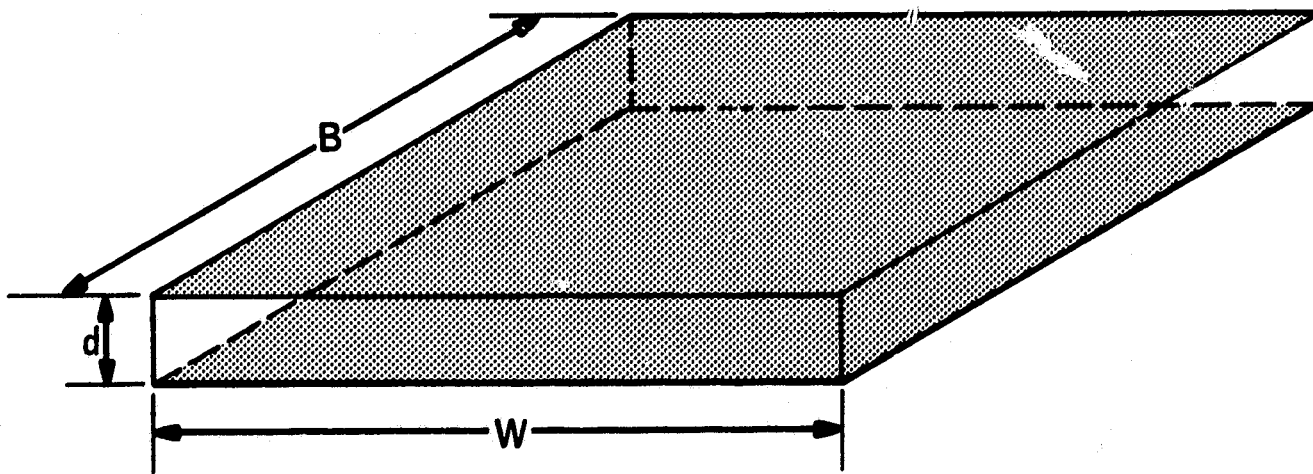
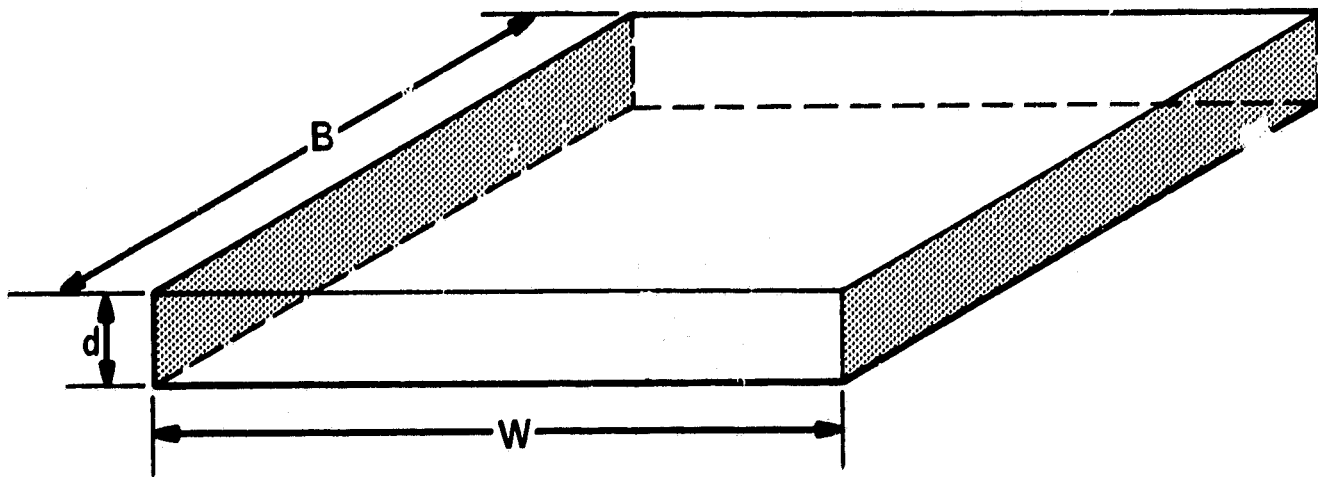
$$\frac{V}{d^2} = \frac{10}{(10^{-4})^2} = 10 \times 10^8 \text{ volts cm}^{-2}$$

This comparison indicates that an order of magnitude in gain can be realized by the use of the volume mode for the extreme case where the operating voltage approaches the breakdown voltage.

To obtain a highly resistive photoconductor, both the resistivity,  $\rho$ , and the element dimensions must be considered. If, for example, the element dimensions are selected to be 1 x 1 mil<sup>2</sup> with a 1 micron thickness, the resistance for the surface and volume mode configurations can be compared. (See Figure 1).

$$\text{For the surface mode, } R = \rho \frac{L}{Wd} = \frac{2.5 \times 10^{-3}}{2.5 \times 10^{-3} \times 10^{-4}} = 10^4 \rho$$

## PHOTOCONDUCTOR CONFIGURATIONS



$$\text{For the volume mode, } R = \rho \frac{d}{WL} = \frac{10^{-4}}{(2.5 \times 10^{-3})^2} = 16 \rho$$

It can be seen that the resistance in the surface mode is approximately three orders of magnitude higher than that of the volume mode.

The parameter,  $\rho$ , used in the above equations can represent the resistivity for a given level of optical excitation or it can represent the resistivity for the dark condition. Since the threshold of operation is defined as that level where the photocurrent equals the dark current, the surface mode of operation permits the sensing of stars with a weaker intensity.

Resolution in one axis of a star tracker associated with a spin stabilized vehicle is determined by the necessary length of exposure during the circular revolution of the detector strip. The integration of signal during successive revolutions can enhance this signal. However, the ultimate limitation in the system is the increments of energy transferred by the photoconductors to the ferroelectric elements during one cycle. Resolution in the other axis is ultimately limited by masking techniques as discussed above.

It is possible to obtain some estimate of signal magnitude derived from a photoconductive element based upon the value of photon irradiance from a star such as Alpheratz, as computed in Appendix II ( $7.8 \times 10^4 \text{ photons sec}^{-1} \text{ cm}^{-2}$ ).

The output signal from a cadmium sulfide photodetector may be expressed as

$$i_s = \frac{V}{R} = \frac{V \sigma A_0}{d}$$

$$\text{since } \sigma = F \tau e u \text{ ohm}^{-1} \text{ cm}^{-1} \quad \text{where } F = \frac{\phi}{V_0}$$

$$i_s = \tau e u \frac{V \phi}{d^2} \quad \text{or}$$

$$i_s = \tau e u \frac{\phi A_0 V}{d^2}$$



where

- e = electronic charge,  $1.6 \times 10^{-19}$  coulombs
- $\tau$  = lifetime of free carrier,  $10^{-2}$  sec TMC material
- u = mobility,  $1.5 \times 10^2$  cm<sup>2</sup> volt<sup>-1</sup> sec<sup>-1</sup> TMC material
- $\phi$  = photon irradiance,  $7.8 \times 10^4$  photons sec<sup>-1</sup> cm<sup>-2</sup> from Appendix II
- A = collecting area of telescope, assume 44 cm<sup>2</sup>
- $t_o$  = transmission of telescope, assume 0.5
- V = applied voltage, assume 1 volt
- d = electrode gap, assume  $1.25 \times 10^{-3}$  cm

$$i_s = 10^{-2} \times 1.5 \times 10^2 \times 1.6 \times 10^{-19} \times \frac{7.8 \times 10^4 \times 44 \times 0.5 \times 1}{(1.25 \times 10^{-3})^2}$$

$$i_s = 1.28 \times 10^{-7} \text{ amperes}$$

If a spin roll rate of 30 revolutions minute<sup>-1</sup> is assumed, the dwell time per degree is

$$\frac{30 \text{ rev min}^{-1}}{60 \text{ seconds}} = 0.5 \text{ rev sec}^{-1}$$

$$\frac{2000 \text{ milliseconds rev}^{-1}}{360 \text{ degrees}} = 5.5 \text{ ms degree}^{-1}$$

The amount of charge required by a 1 mil<sup>2</sup> ferroelectric element such as lead titanate zirconate is

$$Q = 2AP_s$$

where

$$A = \text{area in cm}^2, 6.25 \times 10^{-6} \text{ cm}^2$$

$$P_s = \text{Spontaneous polarization, } 40 \times 10^{-6} \text{ coulomb cm}^{-2}$$

$$\begin{aligned} Q &= 2(6.25 \times 10^{-6}) 40 \times 10^{-6} \\ &= 5 \times 10^{-10} \text{ coulombs} \end{aligned}$$

The amount of charge produced by the photoconductor during an exposure that occurs in a 1 degree of revolution

$$\begin{aligned} Q &= i_s t \\ &= 1.28 \times 10^{-7} \times 5.5 \times 10^{-3} \\ &= 7.05 \times 10^{-10} \text{ coulombs} \end{aligned}$$

it can be seen that this amount of charge is sufficient to fully saturate the ferroelectric element during one exposure time.

#### IV. READOUT TECHNIQUES

Electronic readout of the TMC multielement detector strip can be executed by means of a thin film commutator. A voltage pulse of the opposite polarity to the exposure or write pulse is applied sequentially to the ferroelectric crystals associated with each detector element. A 50 stage electronic commutator is required to accomplish readout of the complete detector strip. Preliminary studies on commutator techniques have indicated a desirable commutator configuration based on thin film transistors that will allow the use of batch fabrication techniques. These thin film field effect transistors employ the same cadmium sulfide-cadmium selenide (CdS-CdSe) materials that have been developed for use in the detector strip.

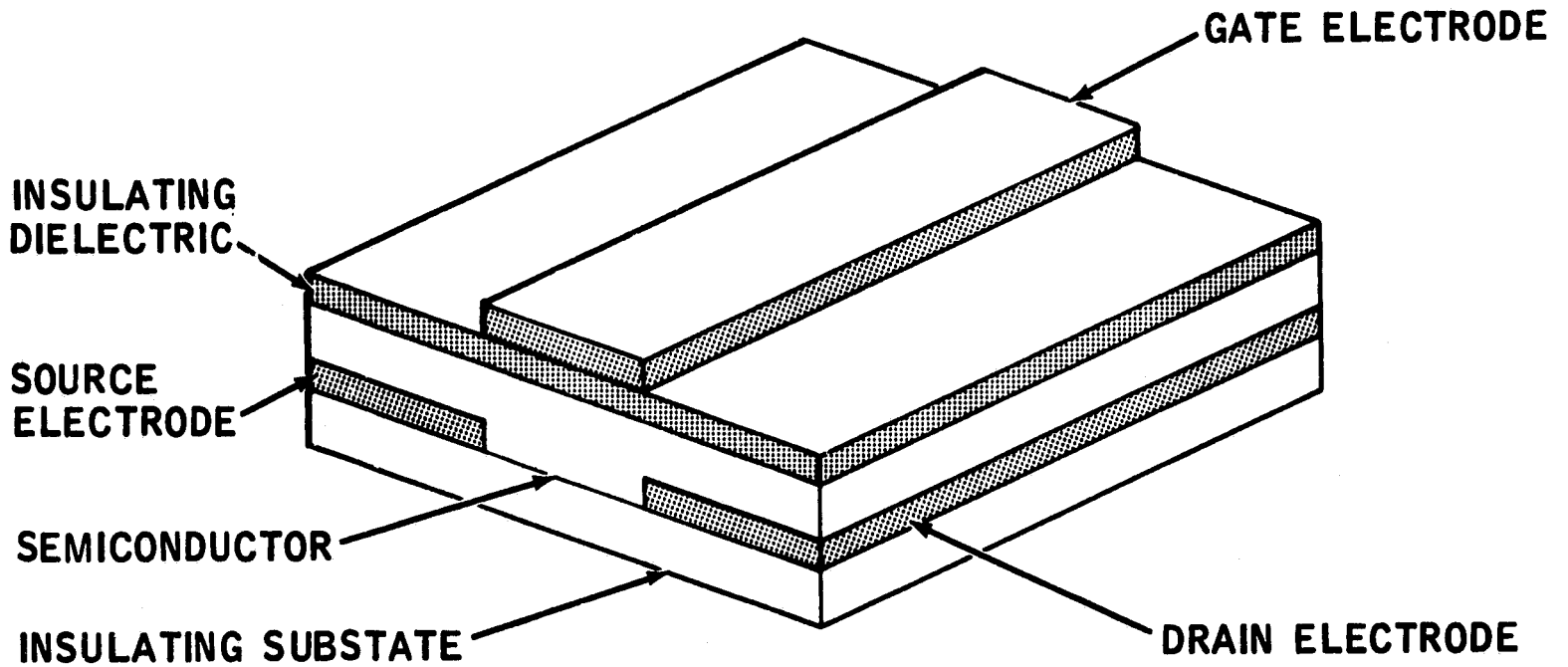
##### A. Theory

The insulated gate field effect transistor (TFT) developed at Marquardt is a semiconductor device in which the conductivity between two electrodes is modulated by the induction of charge into the device through a third insulated electrode. The TFT differs from conventional field effect devices in the use of small dimensions and the choice of wide band gap materials such as CdS-CdSe as the semiconductor. With this insulating or semi-insulating material of high resistivity, the current flow is space charge limited. The thermally-generated carrier density proves to be small compared to the density of majority carriers which can be injected into the material from an electrode thus providing a low noise figure. The specific CdS-CdSe material must have a high mobility, a very low trap density or crystalline defect concentration which imposes stringent requirements on the processing techniques. In conjunction with other programs, Marquardt has developed fabrication techniques which can meet these requirements.

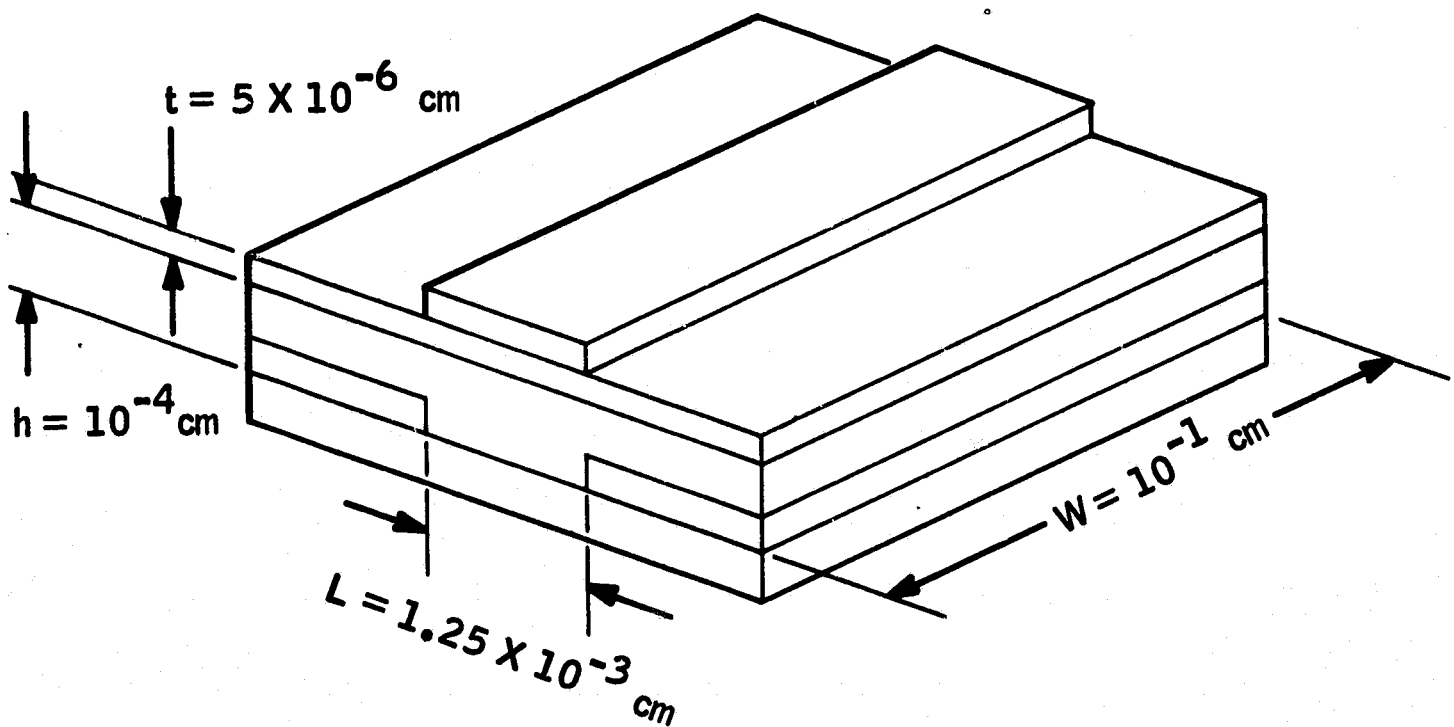
The TFT is constructed with three electrodes; a gate electrode separated from the semiconductor by a thin insulator and two low resistance ohmic contacts to the semiconductor film, or the source and drain electrodes. This thin film structure is shown in Figure 2 along with identification of the various electrodes and the structure dimensions.

The control mechanism is illustrated in Figure 3a. With a positive gate potential, positive charges on the electrode side of the insulator induce a corresponding negative charge at the semiconductor side. As the voltage is increased, the positive charge at the gate is increased and the negative charge in the semiconductor is increased with a proportional increasing change in the conductivity. The current flow from the drain to the source thus will be "enhanced" by

## TFT STRUCTURE AND DIMENSIONS

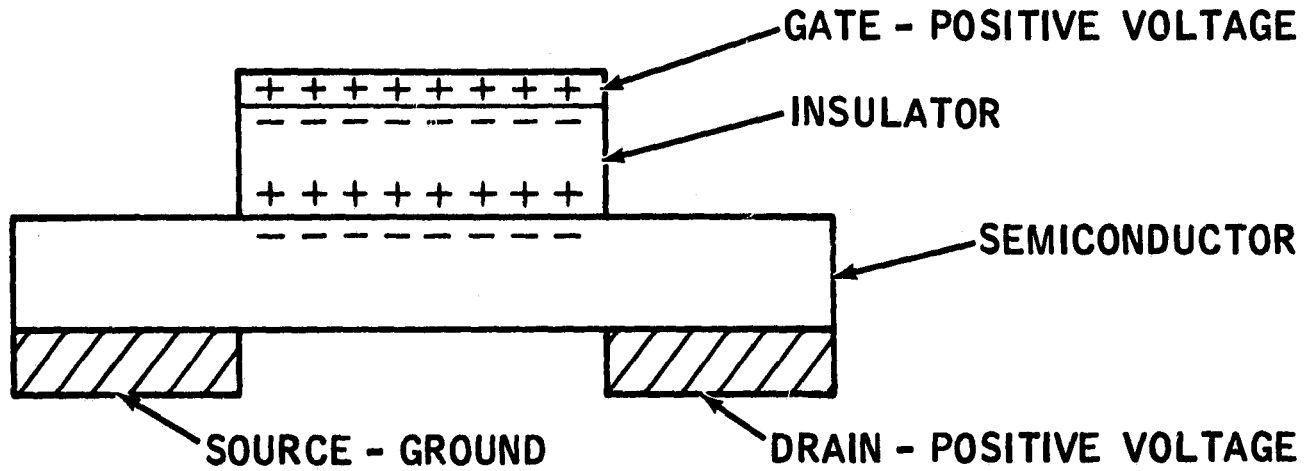


A. STRUCTURE

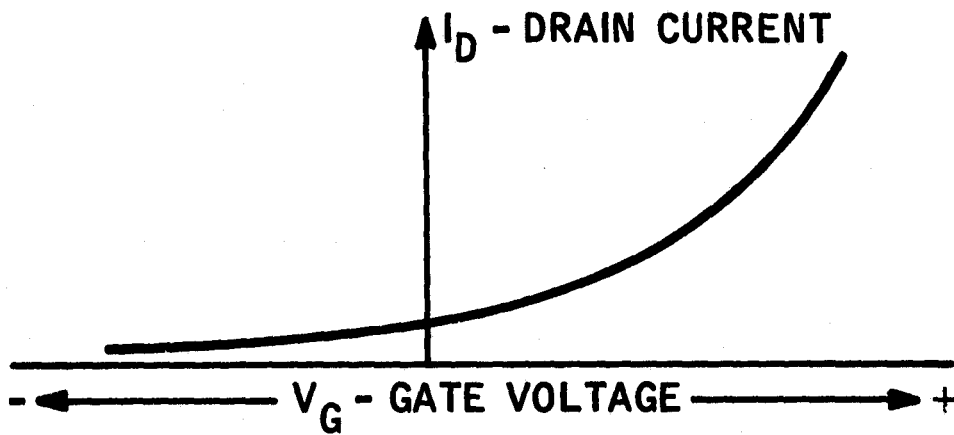


B. DIMENSIONS

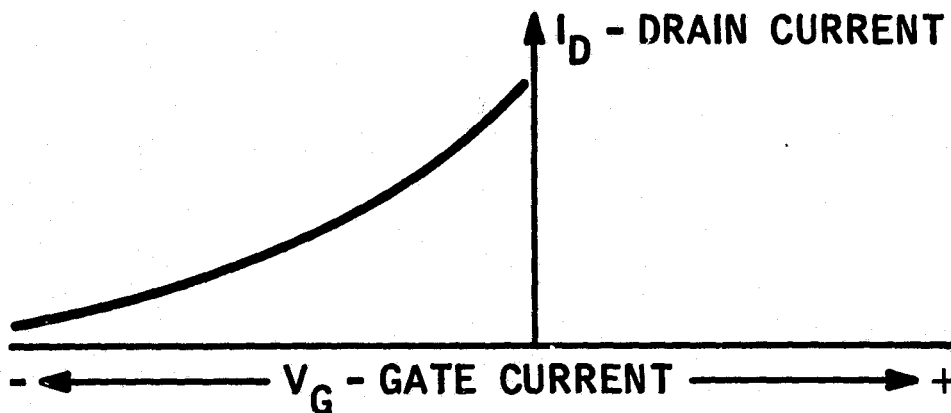
## CONTROL MECHANISM AND CHARACTERISTICS



A. CHARGE INDUCEMENT



B. ENCHANCEMENT MODE



C. DEPLETION MODE

the applied gate potential and the device is said to work in the "enhancement" mode. An increase of a negative gate voltage decreases the drain current in the "depletion" mode. Typical voltage-current relationships are indicated in Figures 3b and 3c.

With a knowledge of device dimensions and the material properties, it is possible to obtain some estimate of the transconductance, the gain-bandwidth product, and the change in conductivity which provide a measure of device performance.

The gate capacitance,

$$C_g = \frac{KWL 10^{-12}}{4 \pi t}$$

where  $W$  = the width of the semiconductor,  $10^{-1}$  cm  
 $L$  = the source-drain electrode gap,  $1.25 \times 10^{-3}$  cm  
 $t$  = the insulator thickness,  $5 \times 10^{-6}$  cm  
 $K$  = dielectric constant, value of 4 for silicon dioxide

$$C_g = \frac{(4)(10^{-1})(1.25 \times 10^{-3})10^{-12}}{4 \pi 5 \times 10^{-6}} 10^{-11} \text{ farad}$$

The transconductance,

$$g_m = \frac{uC_g V_d}{L^2}$$

where  $V_d$  = the drain voltage. Select 5 volts  
 $u$  = the semiconductor mobility,  $1.5 \times 10^2 \text{ cm}^2 \text{ volt}^{-1} \text{ sec}^{-1}$  for TMC CdS-CdSe material

$$g_m = \frac{1.5 \times 10^2 10^{-11} \times 5}{1.5 \times 10^{-6}}$$

$$= 5 \times 10^{-3} \text{ amperes volt}^{-1}$$

The gain-bandwidth product is

$$GB = \frac{gm}{2\pi C_g}$$

$$\frac{5 \times 10^{-3}}{2\pi \times 10^{-11}} = 73 \text{ megahertz}$$

For each volt of gate voltage applied, the amount of charge introduced into the semiconductor is

$$Q = V_g C_g = 1 \times 10^{-11} \text{ coulombs}$$

If the approximate assumption is made that this charge is evenly distributed throughout the semiconductor, the total change in carriers is

$$\frac{Q}{e} = \frac{10^{-11}}{1.6 \times 10^{-19}} = 6 \times 10^7 \text{ carriers n}$$

Since the conductivity,  $\sigma = neu$ , this represents a change in conductivity

$$\begin{aligned} \Delta\sigma &= 6 \times 10^7 \times 1.6 \times 10^{-19} \times 1.5 \times 10^2 \\ &= 1.44 \times 10^{-9} \text{ ohm}^{-1}\text{-cm}^{-1} \end{aligned}$$

Since the resistivity,  $\rho = \frac{1}{\sigma}$ ,  $\Delta\rho = 6 \times 10^8 \text{ ohm-cm}$

Since the resistance,  $R = \rho \frac{W}{Lh}$

$$\begin{aligned} \Delta R &= \frac{6 \times 10^8 \times 10^{-1}}{1.25 \times 10^{-3} \times 10^{-4}} \\ &= 4.8 \times 10^{14} \text{ ohms} \end{aligned}$$

Since the charge must be integrated over the length of the semiconductor, this estimate is quite high but it indicates the wide control of the drain current.

## B. Experiments

To obtain specific component values for a thin film commutator, a breadboard model using discrete components was constructed and tested. Based upon these experimental tests it was determined that, for a scan rate of 2 kilohertz, a drain resistor value of 100K ohms with a capacitance of 0.01 microfarad would provide adequate current to switch a fully charged ferroelectric element of about 5 mils square without interrupting the scanning sequence. (See Figure 4).

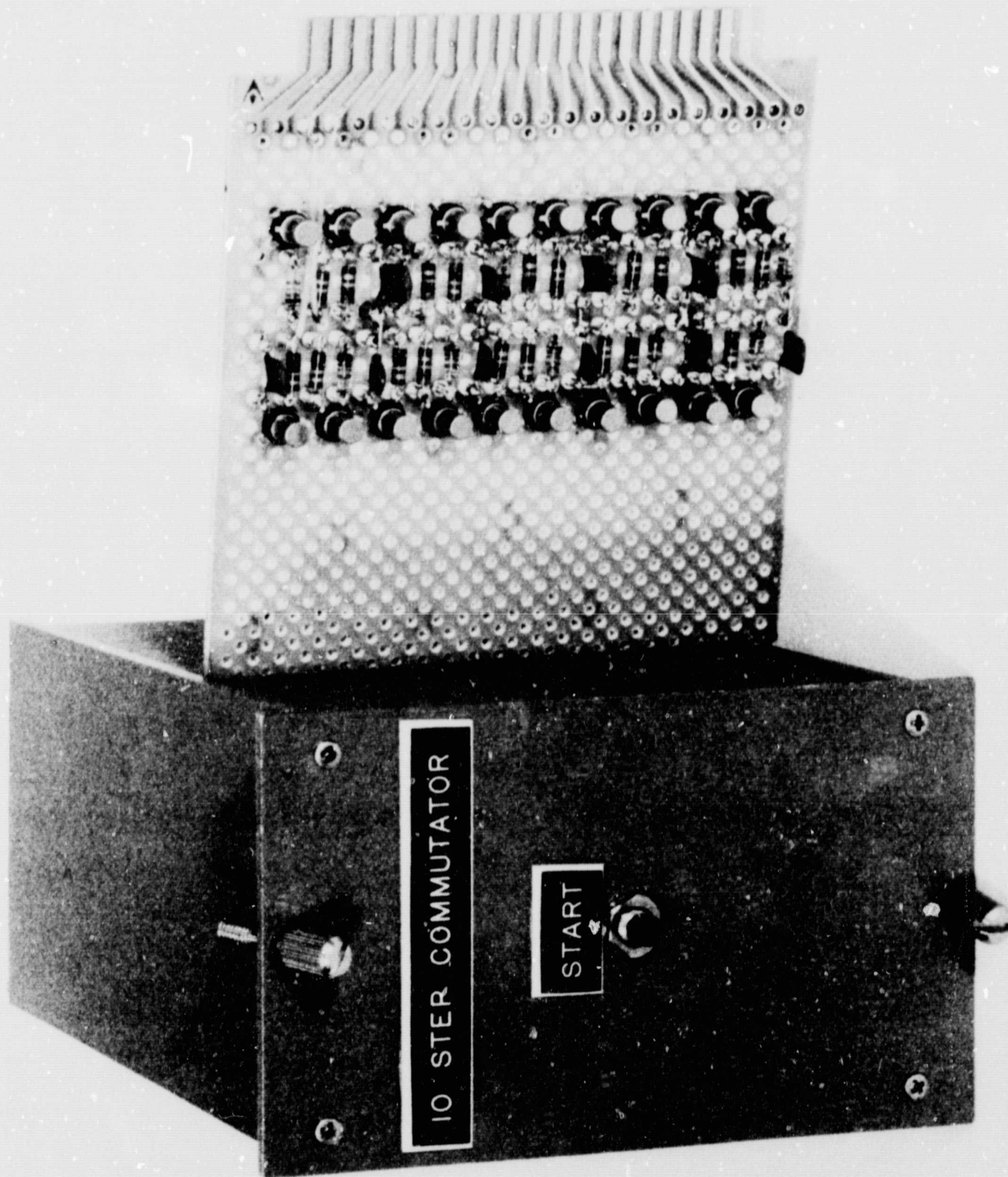
The commutator element sizes were calculated and the materials were selected based on this data. The TFT dimensions are shown in Figure 2, the equivalent circuit is shown in Figure 5, and Figure 6 indicates the interconnection of the TFT electrodes for a section of the 50-stage commutator.

In operation, a positive start pulse is applied to the gate of the first triode (Q1). A positive pulse at the gate of the triode causes that unit to conduct heavily (high current amplification) and the output voltage at the drain electrode to be zero voltage (equal to the source potential). Thus Q1 is highly conducting and the voltage applied to Q2 is essentially zero volts. Q2 is therefore cut off and the drain voltage current through R2 charges capacitor C1 during the period in which the start pulse and drain voltage are "on". The output of Q2, besides charging C1, is also connected to the first element of the detector strip through the electrode fanout to provide the switching voltage and current to the first ferroelectric storage element. In order to sequence the commutator to the second detector element, the drain voltages are divided into two sets of voltage with a 180° phase difference. Thus, the drain voltage is applied first to all odd number stages and then to all even number stages. Removing voltage from the drains of Q1 and Q2, removes voltage from the first detector element. In turn, drain voltage is then applied to Q3 and Q4 and the sequence repeats due to the charge stored on C1 during the previous cycle which applies a positive potential to the gate of Q3. Readout voltage is thereby applied to the second detector element.

Several thin film commutators were fabricated by thin film techniques using dimensions outlined above. The various thin film layers were vacuum deposited on Corning 7059 glass substrates. Vacuum evaporated chromium electrodes established the source, gate, and drain geometries. A TMC developed CdS-Se material provided the semiconductor layer. A mixture of silicon dioxide (SiO<sub>2</sub>) and dysprosium (Dy<sub>2</sub>O<sub>3</sub>) was used for the insulating layer that forms the gate input. Tellurium diodes provided the necessary discharge impedances. Figure 7 indicates the component layout in one of the deposited circuits.



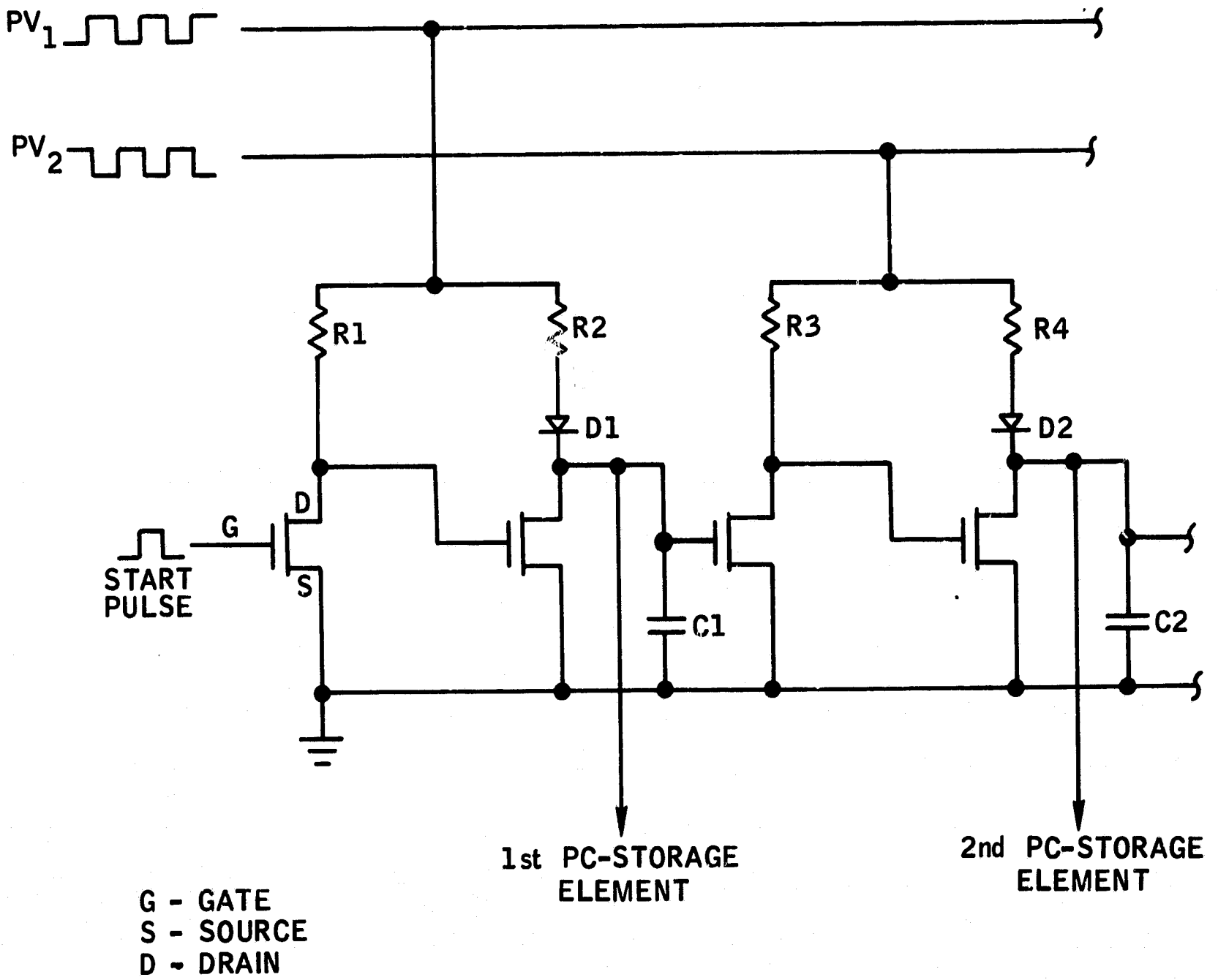
DISCRETE ELEMENT COMMUTATOR






R-26,869  
Neg. 9385-7

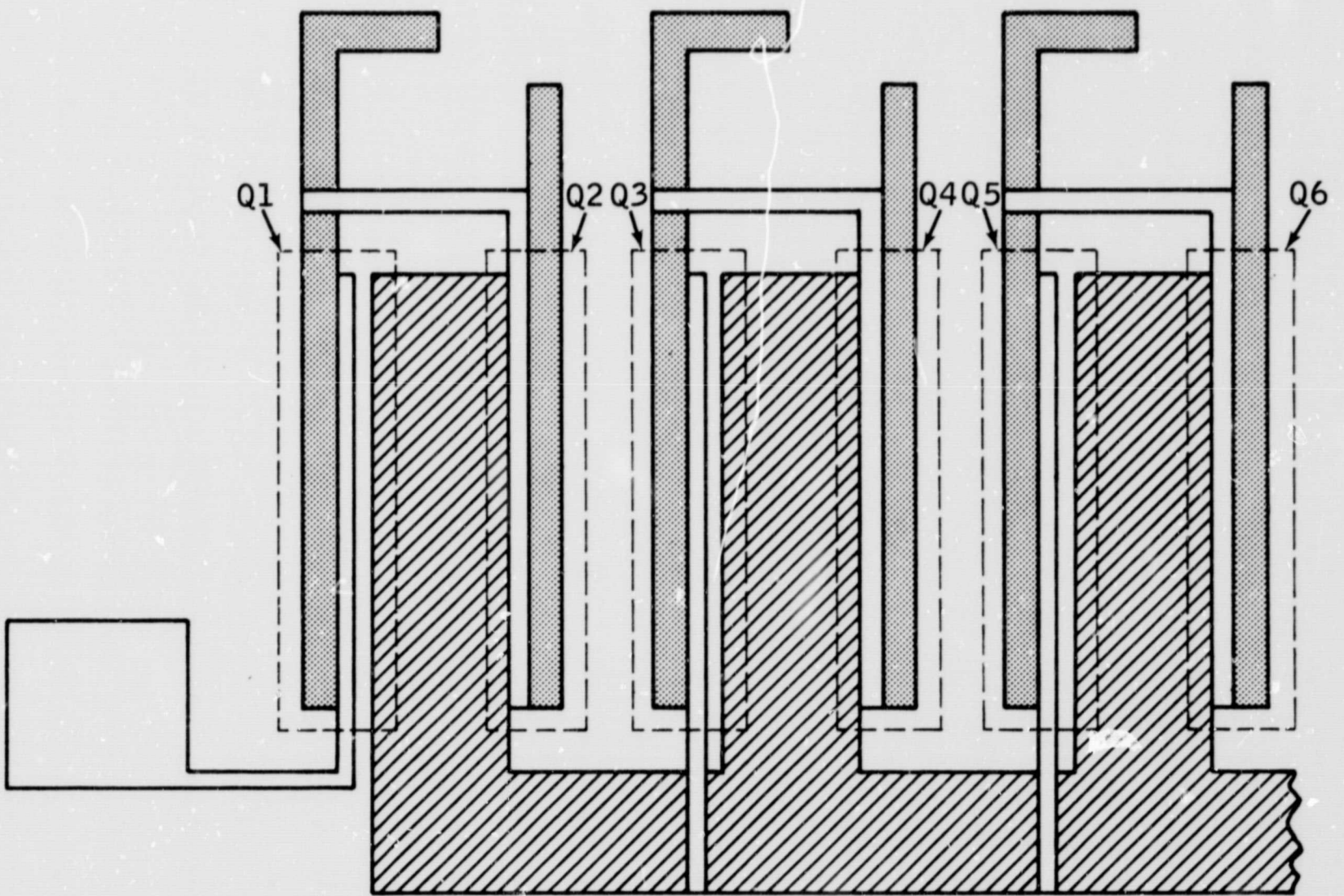
Figure 4

### TFT EQUIVALENT CIRCUIT



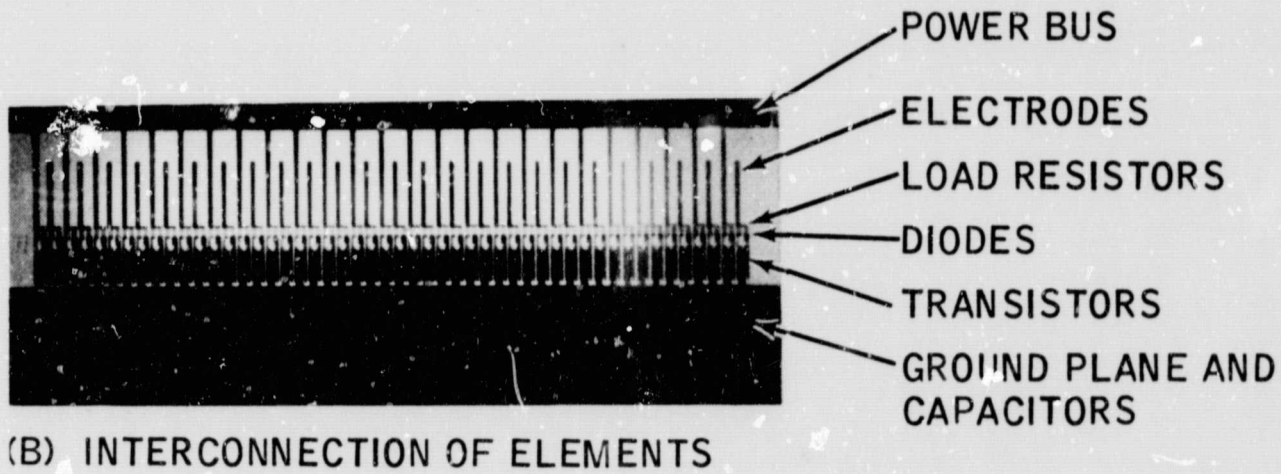
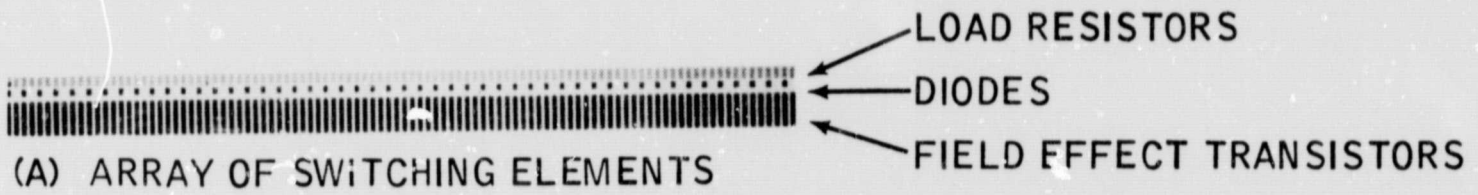
# COMMUTATOR ELECTRODE CONFIGURATION

-  GATE ELECTRODE
-  SOURCE ELECTRODE
-  DRAIN ELECTRODE





TYPICAL COMPONENT PATTERN OF A 50 LINE COMMUTATOR  
(SIZE x4)



Experimental evaluation of individual stages indicated a typical gate input capacitance of 30 picofarads and a transconductance of 2000 micro amperes per volt which provided a reasonable correlation with calculated values.

Several drift problems were encountered when the 50-stage circuit was tested. This type of instability has been encountered by other experimenters in the field. The drift was evidenced only in certain stages of the circuit. The scope of the contract did not permit a full scale investigation.

V. THIN FILM DETECTOR STRIP EVALUATION

As described in NAS5-10193 Final Report, a series of tests were conducted to assess the integration capability of the sensor/storage elements to integrate pulsed light signals. The photoconductor and ferroelectric elements used in these tests were mounted in semiconductor type TO-5 containers for convenience in evaluation. During this phase, essentially the same evaluation was performed on a small thin film model of the star detector strip.

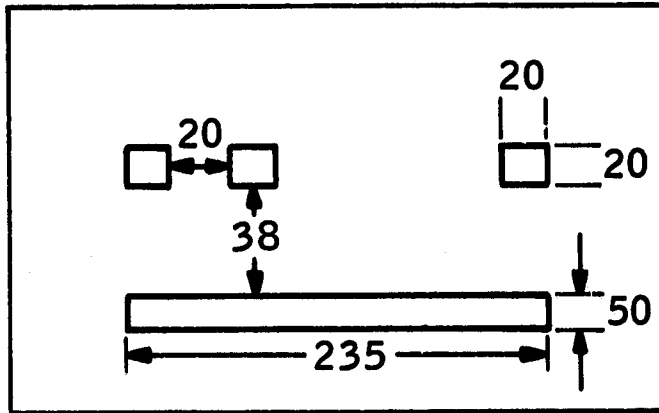
This detector strip was fabricated by first electroding a 4 mil layer of a lead titanate zirconate ferroelectric with a solid gold electrode and a linear array of six 20 x 20 mil dot electrodes on opposite sides. A 4.0 micron thick layer of cadmium sulfide-cadmium selenide (CdS-CdSe) photoconductor material was vacuum deposited on this assembly and subsequently heat treated. A 50 gold bar was then evaporated on the material to serve as a common electrode. The dimensions of the array and a cross-section are indicated in Figure 8.

Preparatory to model evaluation, the spinning star simulation equipment which provides a rotating spot of light was modified. (See NAS5-10193 Final Report). The modified star simulator will permit the calibration of each element of the star detector strip as well as its evaluation under simulated star images of specific star patterns and color index. Figure 9 depicts the simulator configuration. It consists of a large (36 inch diameter) simulator disc which carries a 5 degree star pattern aperture and 24 calibration holes (0.040"). The disc is rotated at a constant speed of 30 rpm. A variable filter wheel (for simulating star color indices) is attached between the lamp housing and simulator disc.

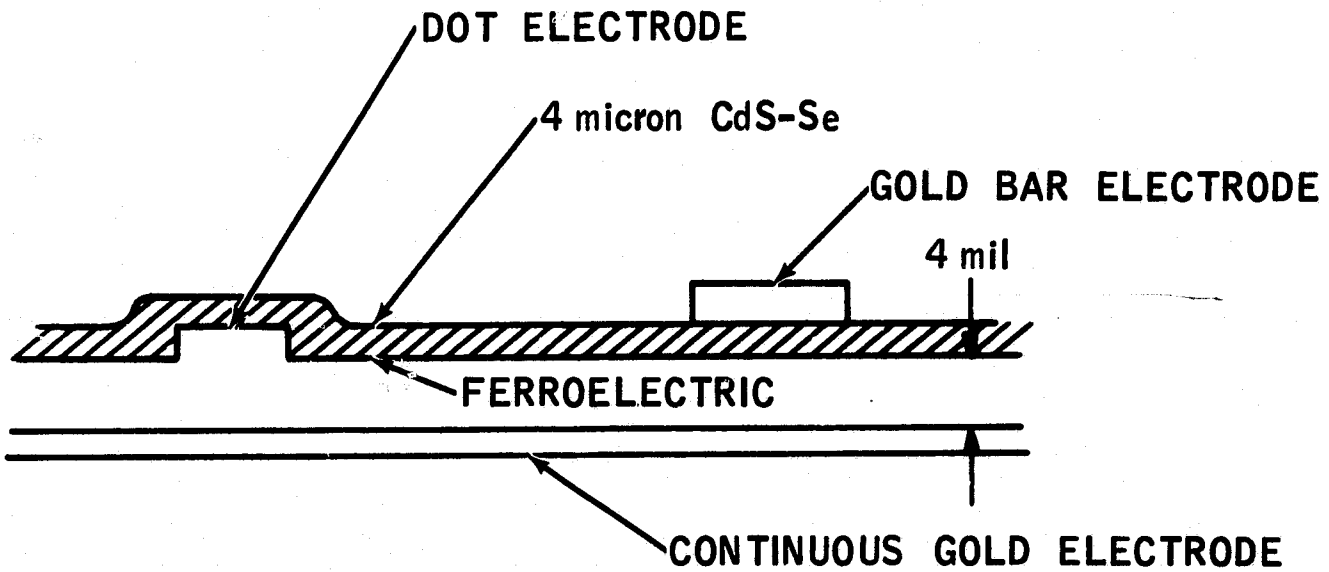
Attached to the simulator disc is a second cover disc that permits the selection of either the calibration holes or star pattern aperture. A convenient means of positioning these discs relative to each other is provided by way of three "wing nuts".

For setup and calibration of the star detector strip, the simulator cover disc is positioned such that the 24 calibration holes are in their open position and the star pattern aperture is closed. Each element of the star detector can then be individually evaluated to determine its performance capability by moving the sensor strip relative to the optical axis of the holes by means of micrometer adjustments on the strip mount. During star pattern sensing, the star pattern aperture is opened and the calibration holes are closed. For purposes of multiple star image evaluation, templates of star patterns can be mounted in the star pattern aperture selected to reproduce specific spectral and star magnitude characteristics.

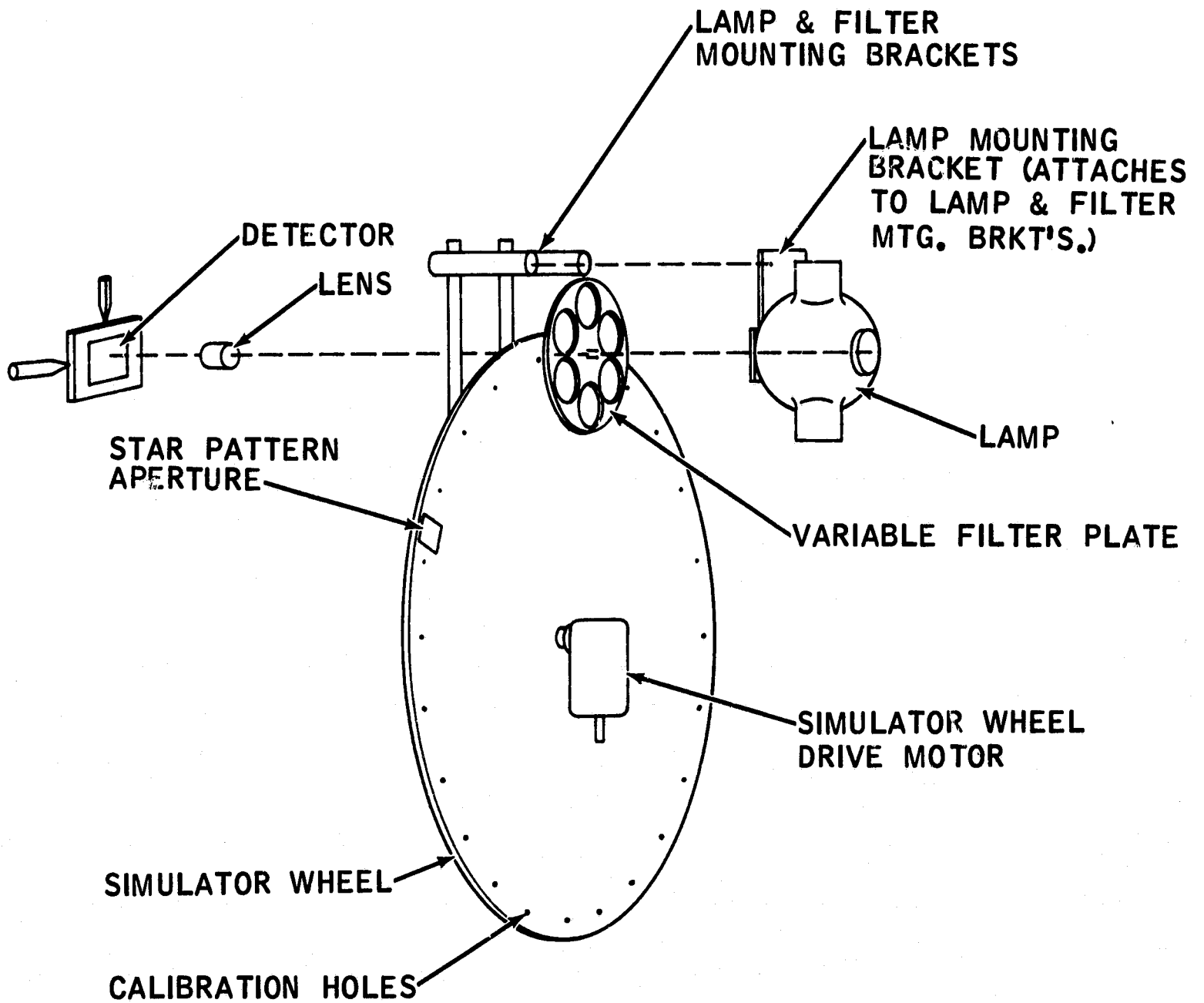
## DETECTOR STRIP GEOMETRY



DIMENSIONS IN mils



## STAR PATTERN SIMULATOR



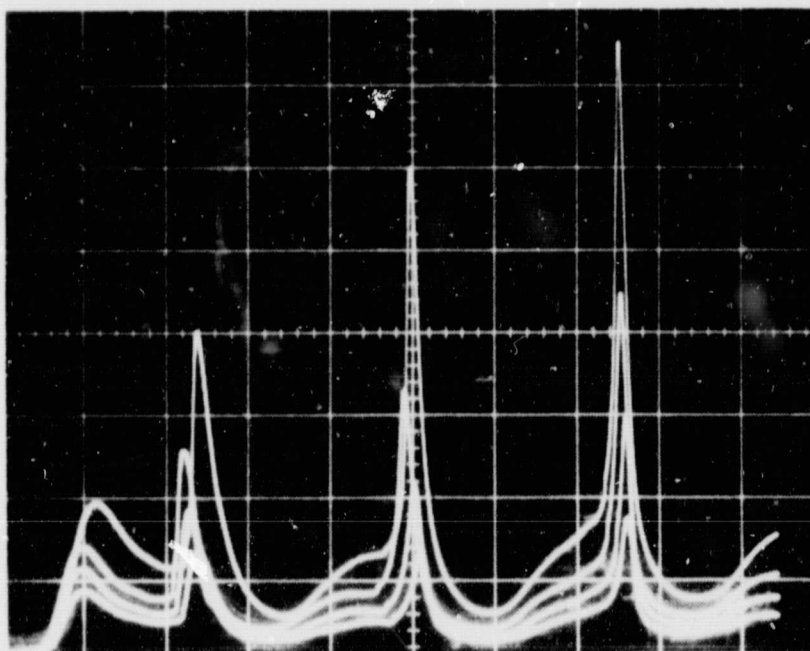


The main objective in model testing was to demonstrate the integration capability of a detector strip fabricated by thin film techniques.

Preparatory to testing, each ferroelectric element was completely polarized by exposing its associated photoconductor to high intensity light with an applied voltage of approximately 80 volts across the photoconductor-ferroelectric combination. For the readin operation, the voltage polarity was reversed and a neutral filter of 6.5% transmittance was placed between the photoconductor elements and the light source to provide an illumination of approximately 80 footcandles. The photoconductors were then subjected to a number of short light pulses. After exposure, the potential was reversed and with the filter removed, the photoconductors were flooded with light for readout. The switching action of three ferroelectric elements is shown in Figure 10. The bottom oscilloscope trace indicates the readout current that occurred after each element had been exposed to one readin light pulse. The second trace shows the readout for two readin pulses. The third trace indicates the effect of four readin light pulses and the top trace exhibits readout after 8 readin pulses.

The significant result is the linearity of stored charge against the number of light pulses when considering individual elements. It is believed that the deviation from element to element is the result of parasitic capacitance.

## DETECTOR STRIP INTEGRATION



VERTICAL = 0.1 volt DIV<sup>-1</sup>  
HORIZONTAL = 20 msec DIV<sup>-1</sup>  
 $R_L = 500 \text{ K}$

## VI. THIN FILM MATERIAL DEVELOPMENT

The fabrication of the Marquardt detector strip and the TFT commutator involve the use of highly refined thin film processing techniques for the preparation of the photoconductor and ferroelectric materials. The material effort during this phase was directed mainly toward the improvement of the film quality of the photoconductor in order to establish the high degree of uniformity needed for a star tracker application.

The extremely low level signal currents which are derived in a star tracker application requires a material that has been processed by techniques that provide uniformity in electrical characteristics by eliminating mechanical defects.

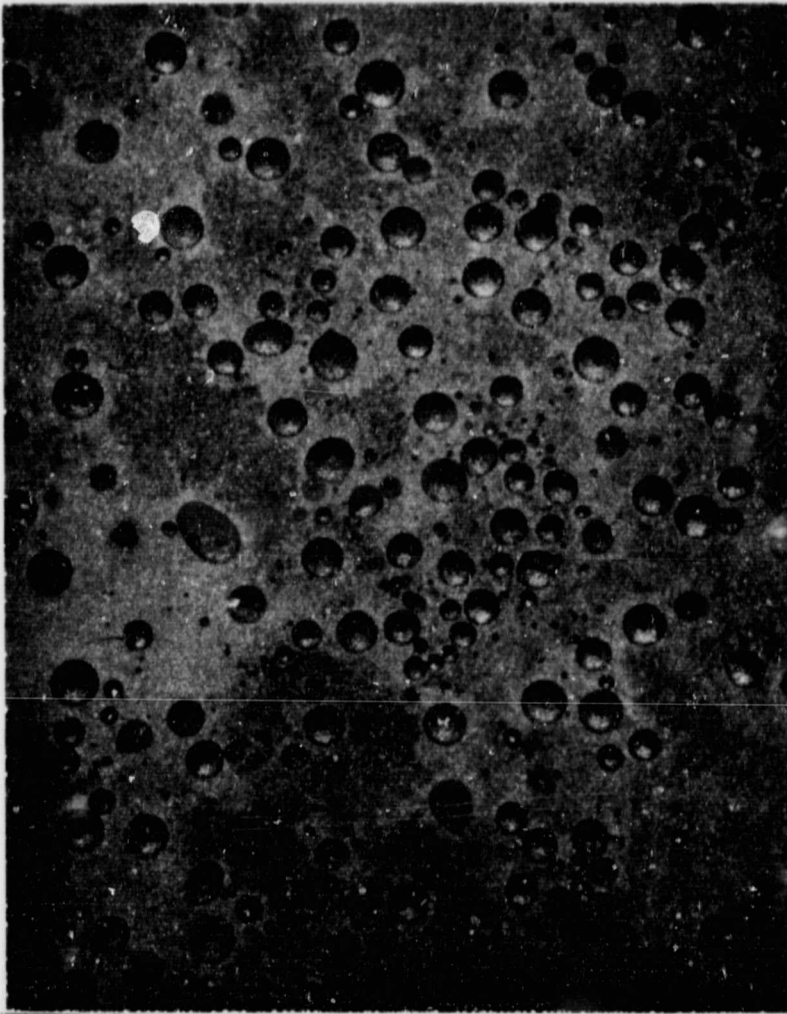
Work was initiated, in conjunction with another program, to determine the possible origin of such mechanical defects which can occur during the various stages of vacuum deposition and post activation of thin film CdS and CdS-Se photoconductive materials. The objective was accomplished by modifying the deposition as well as the post processing techniques.

In the normal processing procedure, a 4.0 micron thick CdS or CdS-Se film is deposited onto a heated 7059 Corning glass substrate. The evaporation temperature is kept between 800°C-900°C. After the deposition of CdS, a layer of copper and a layer of CdCl<sub>2</sub> is deposited over the photoconductor. To transform the amorphous film into a polycrystalline film each individual sample is post heat treated. For this purpose, the photoconductor is heated on a heater strip from room temperature to the crystallization temperature within several seconds.

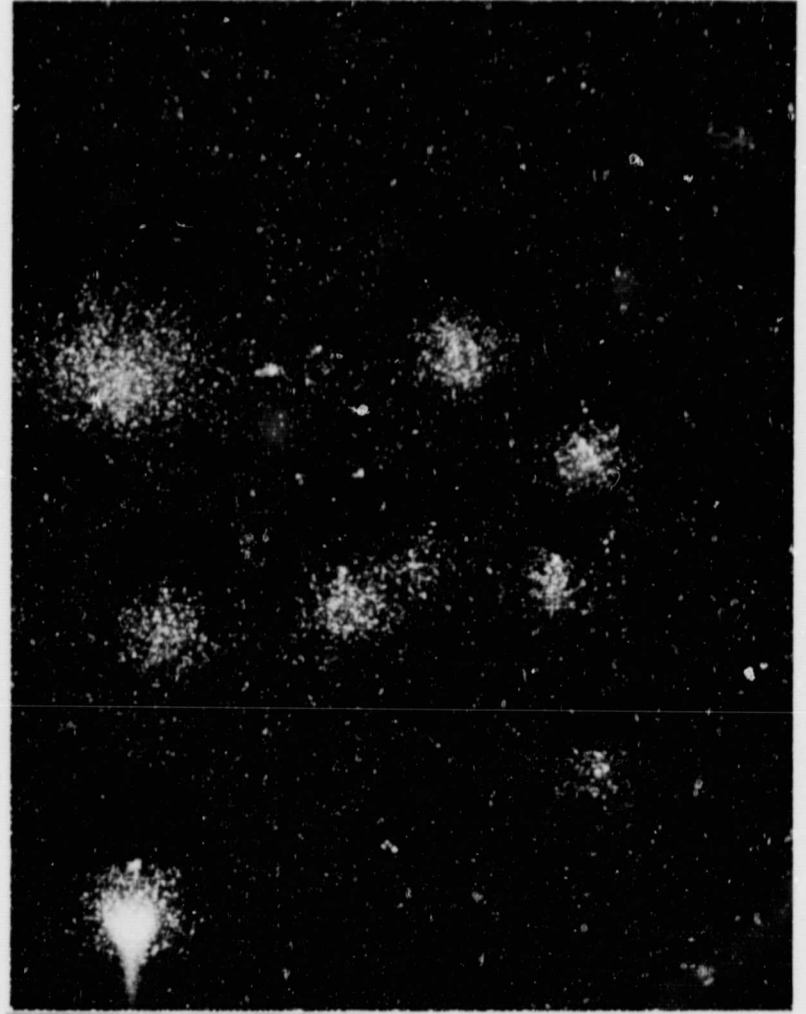
A microscopic examination was made of films obtained by this process. Figures 11a and 11b show the film structure of a typical area under 43X and 430X magnification. By illumination of the film from the bottom and the side, a large number of bubbles become clearly visible over the entire surface area. The average diameter of these bubbles was approximately 60 microns and the bubbles protruded 1 to 2 microns above the surface of the film. To depict the crystalline structure of such films an area free of bubbles was examined with a magnification of 940X. Figure 12a shows that crystals of less than 1 micron size were evident.

To determine the origin of formation of the bubbles, a systematic approach was employed:

PHOTOMICROGRAPH OF SURFACE OF DEPOSITED CdS FILM



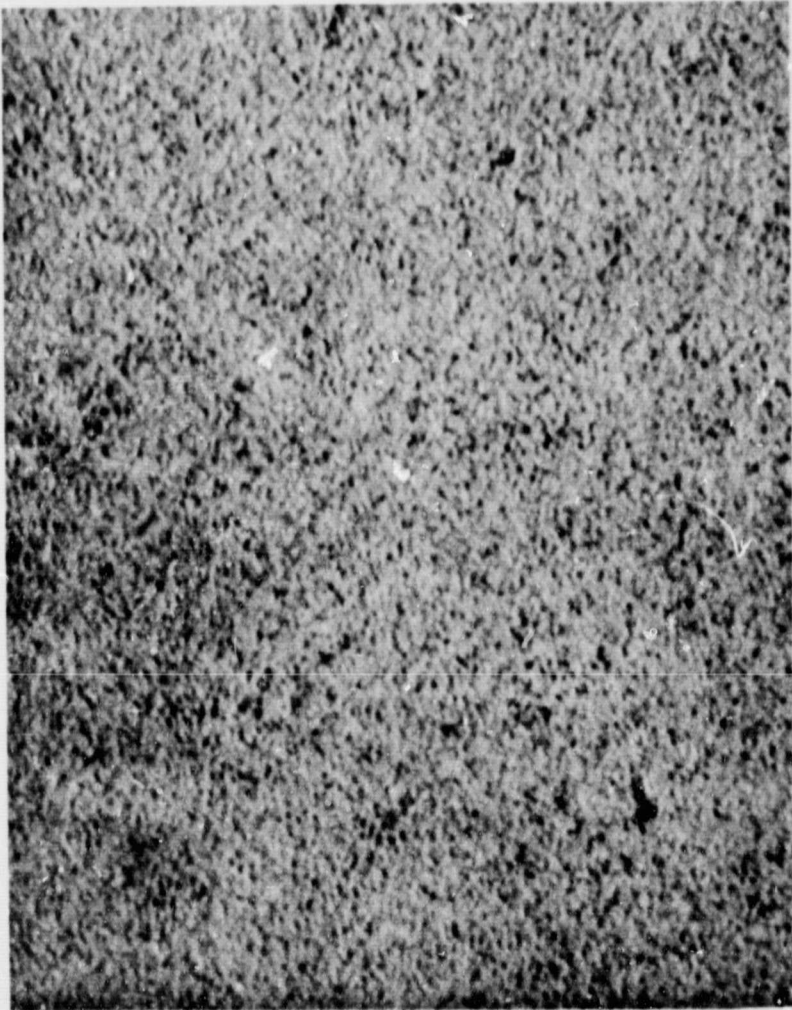
DEPOSITION SEQUENCE: CdS + Cu + Cd Cl<sub>2</sub>  
MAGNIFICATION 43X



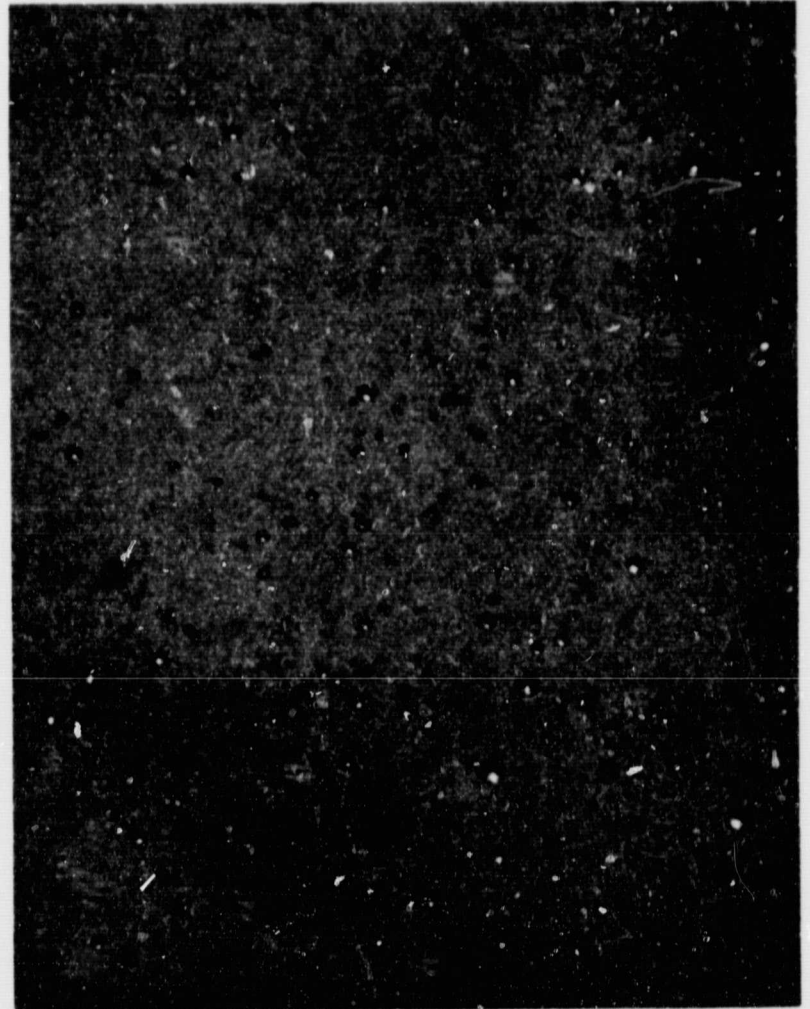
DEPOSITION SEQUENCE: CdS + Cu + Cd Cl<sub>2</sub>  
MAGNIFICATION 430 X



PHOTOMICROGRAPH OF SURFACE OF DEPOSITED CdS FILM



DEPOSITION SEQUENCE: CdS + Cu + Cd Cl<sub>2</sub>  
MAGNIFICATION 940 X



DEPOSITION SEQUENCE: CdS + Cd Cl<sub>2</sub> + Cu  
MAGNIFICATION 43X

- (1) The sequence of evaporation was changed from CdS-Cu-CdCl<sub>2</sub> to CdS-CdCl<sub>2</sub>-Cu. Microscopic investigation of these films indicated that the number of bubbles and the bubble diameter had decreased. A comparison of Figure 12b with Figure 12a shows that the average diameter had decreased by a factor of 3 or 4
- (2) In another example, the layer of copper was deleted. As can be seen, Figure 13a at 43X magnification has the same appearance as Figure . The reason for the somewhat smaller number of bubbles might be the particular area of the film selected for examination.
- (3) As a next step, the cadmium chloride layer was deleted, i.e., the sandwich consisted of a layer of CdS with a layer of Cu evaporated over it. It can be clearly seen in Figure 13b that the bubbles have disappeared completely. However, the interference rings indicate that the film was lifting from the substrate. Closer examination of Figure 13b shows that with each interference pattern there is an associated dust particle or some other small piece of material which could have been introduced during or after the evaporation process.
- (4) For the next test, an unprocessed as well as a processed CdS layer was examined. Figure 14a shows the unprocessed CdS layer at 43X magnification. At higher magnification (not shown) neither bubbles nor interference rings were detected but pieces of material of irregular size were visible. Figure 14b shows the same film after activation. Lifting of the films from the substrate is indicated by the interference rings.

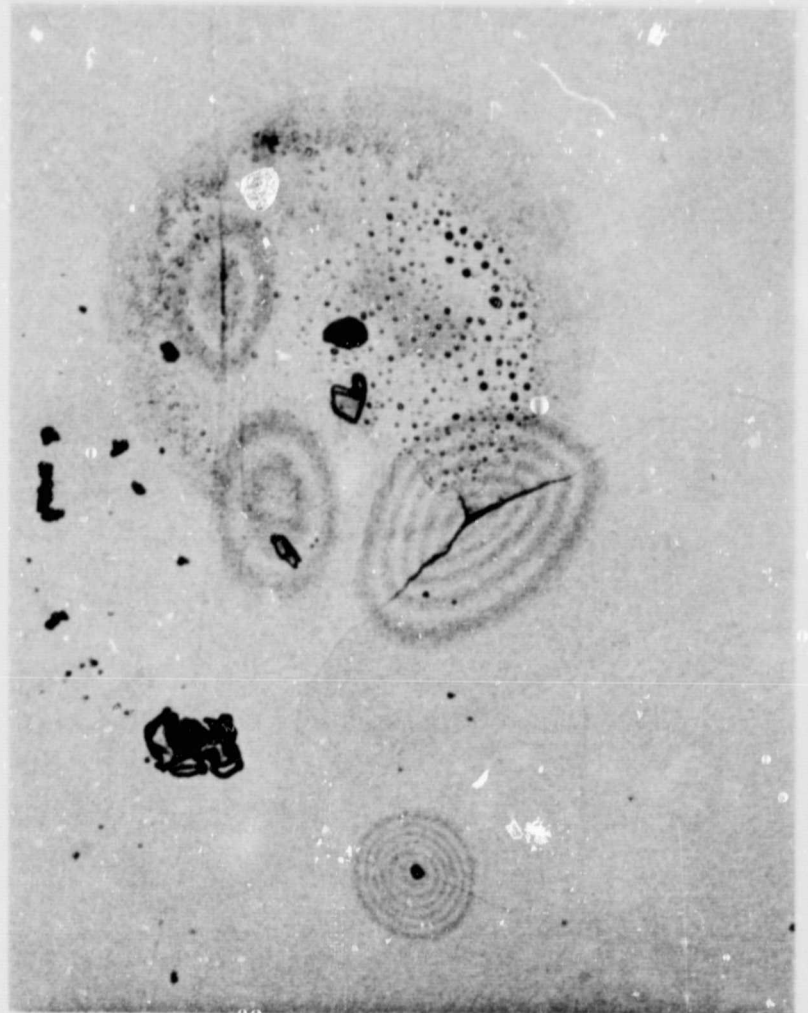
It was concluded from these tests that the bubble formation must be attributed to the introduction of cadmium chloride and it was shown that the diameter and the number of occurrences of bubbles strongly depends upon the stage in the process at which cadmium chloride is introduced into the film.

As a first step toward the elimination of this problem, a CdS layer was again provided with a layer of copper and a layer of cadmium chloride. This sandwich was activated slowly by raising the temperature from room temperature to the crystallization temperature within several minutes. Microscopic examination of such a film revealed a drastic reduction in the number of bubbles. (See Figure 15a). A comparison with Figure shows a marked improvement with respect to the

PHOTOMICROGRAPH OF SURFACE OF DEPOSITED CdS FILM



DEPOSITION SEQUENCE: CdS + Cd Cl<sub>2</sub>  
MAGNIFICATION 43X



DEPOSITION SEQUENCE: CdS + Cu  
MAGNIFICATION 43X

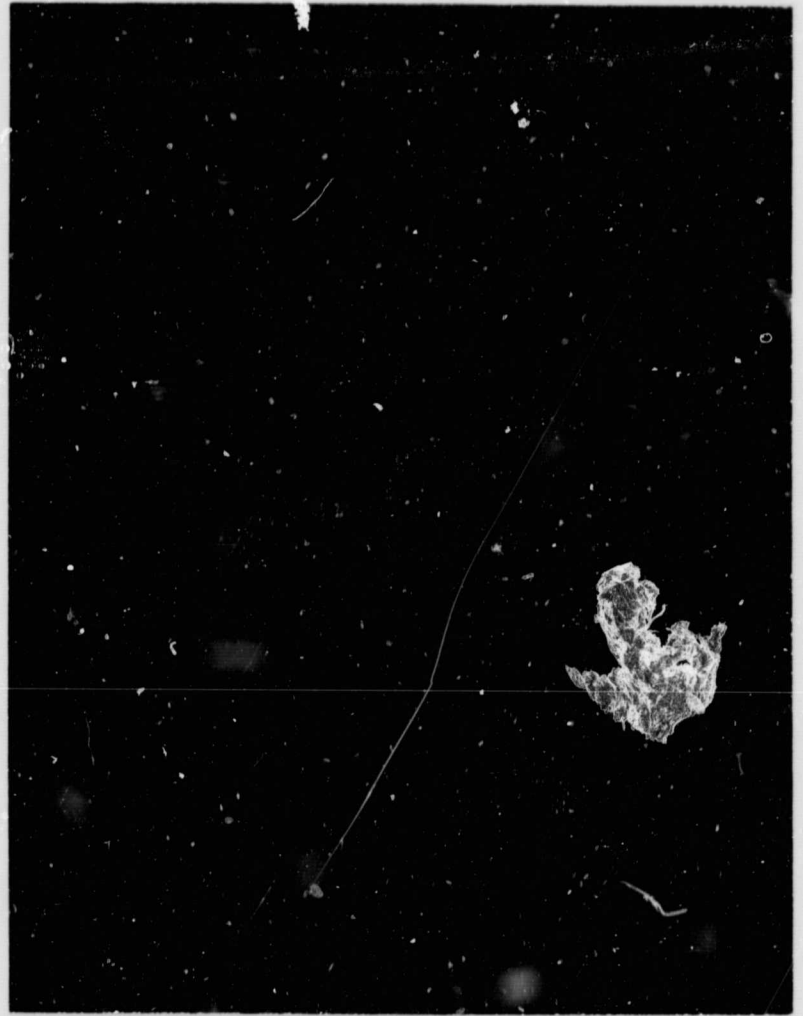


PHOTOMICROGRAPH OF SURFACE OF DEPOSITED CdS FILM



DEPOSITION OF CdS ONLY  
(NOT HEAT PROCESSED)

MAGNIFICATION 43X



DEPOSITION OF CdS ONLY  
(AFTER HEAT PROCESSING)

MAGNIFICATION 43X



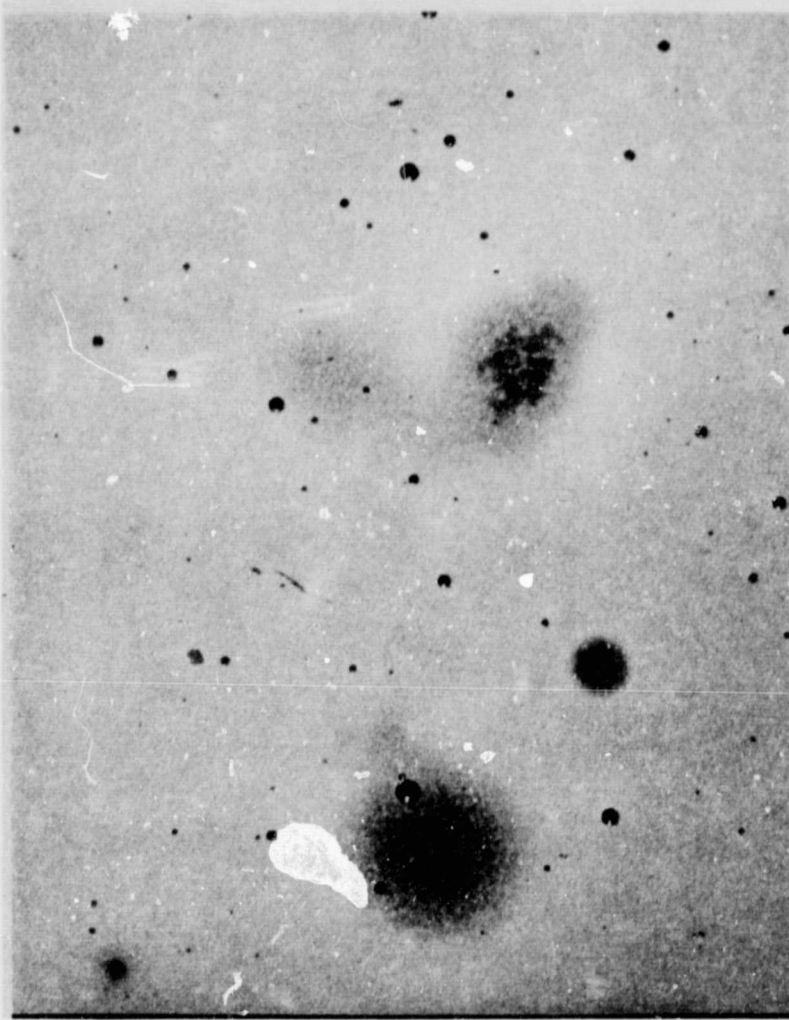
number of bubbles. Spots and dark areas in Figure 15a are most likely caused by spitting of the evaporant from the evaporation sources and foreign matter which settled onto the slide after deposition.

As a second step, the sequence of deposited layers was altered, i.e.,  $\text{CdCl}_2$  was first evaporated onto the glass substrate, followed by a layer of Cu and CdS. The thickness of each film was maintained throughout the experiments. One sample was activated by the previously described method. Figure 15b shows that the film has lifted from the substrate over the entire area. Another sample was then heated very slowly. Microscopic examination of this particular film revealed the complete absence of bubbles as shown in Figures 16a and 16b.

An attempt was made to determine the structural characteristics of the CdS photoconductor obtained by sequentially evaporating  $\text{CdCl}_2$ , Cu, and CdS with subsequent slow heat treatment. Polarizing microscopy, photomicrography, X-ray diffraction, and emission spectrography were used to determine these structural characteristics.

- (1) Polarizing microscopy revealed that the CdS film is a polycrystalline mosaic of apparently randomly oriented crystallites. Since practically no isotropic sections were visible, the presence of the cubic form of CdS can be ruled out. The few isotropic sections that appeared could be explained as alpha or hexagonal CdS crystals with the basal planes parallel to the substrate. High magnification revealed that individual crystals were irregular in shape with the upper edges rounded. Electromicroscopic examination would provide more definite results.
- (2) The photomicrograph shown in Figure 16b exhibits black areas between crystallites which are very opaque to transmitted light. These black areas proved to be metallic globules when viewed under the illumination provided by a strong grazing light. Figure 17a, which was taken with transmitted light and at 940 magnification, shows the crystallite size in horizontal cross section. The size ranges from 1 to 6 microns. The random orientation of crystals in the horizontal plane is shown by transmitted polarized light ( $84^\circ$ ) in Figure 17b.
- (3) X-ray diffraction confirmed that, after recrystallization of the films, the crystallites are of the alpha or hexagonal structure. The crystallites are preferentially

PHOTOMICROGRAPH OF SURFACE OF DEPOSITED CdS FILM



DEPOSITION SEQUENCE: CdS + Cu + Cd Cl<sub>2</sub>  
(SLOW HEAT PROCESSING)

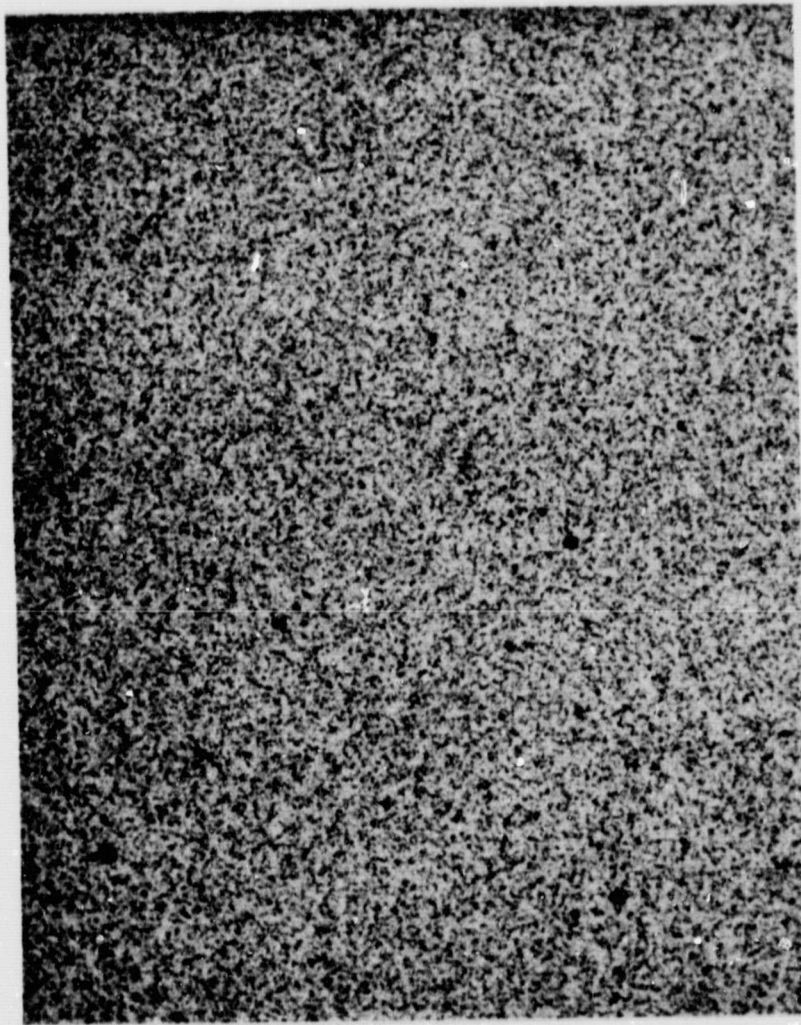
MAGNIFICATION 43X



DEPOSITION SEQUENCE: Cd Cl<sub>2</sub> + Cu + CdS  
(FAST HEAT PROCESSING)

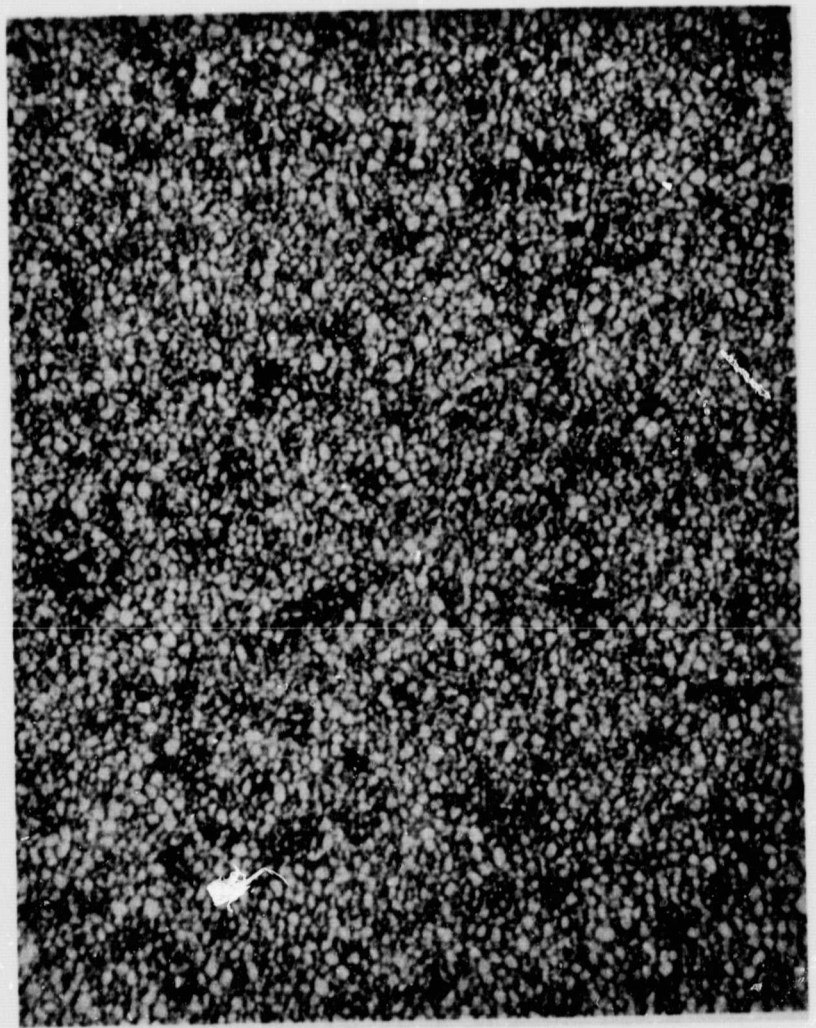
MAGNIFICATION 43X

PHOTOMICROGRAPH OF SURFACE OF DEPOSITED CdS FILM



DEPOSITION SEQUENCE: Cd Cl<sub>2</sub> + Cu + CdS  
(SLOW HEAT PROCESSING)

MAGNIFICATION 43X

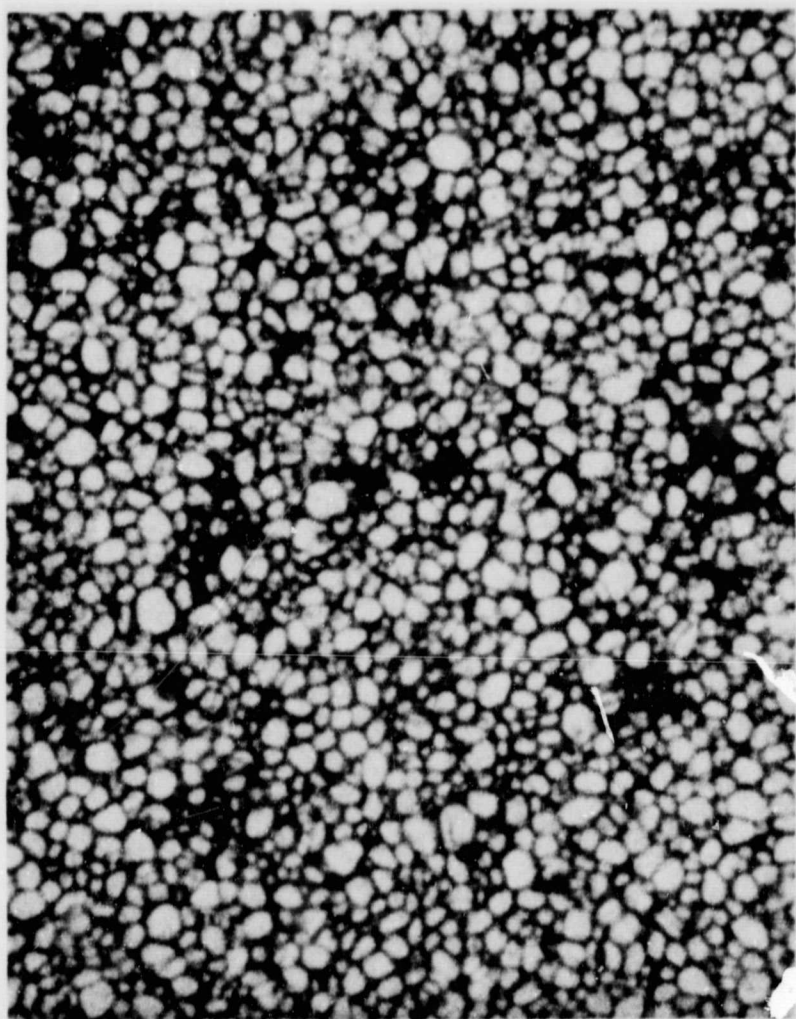


DEPOSITION SEQUENCE: Cd Cl<sub>2</sub> + Cu + CdS  
(SLOW HEAT PROCESSING)

MAGNIFICATION 430 X

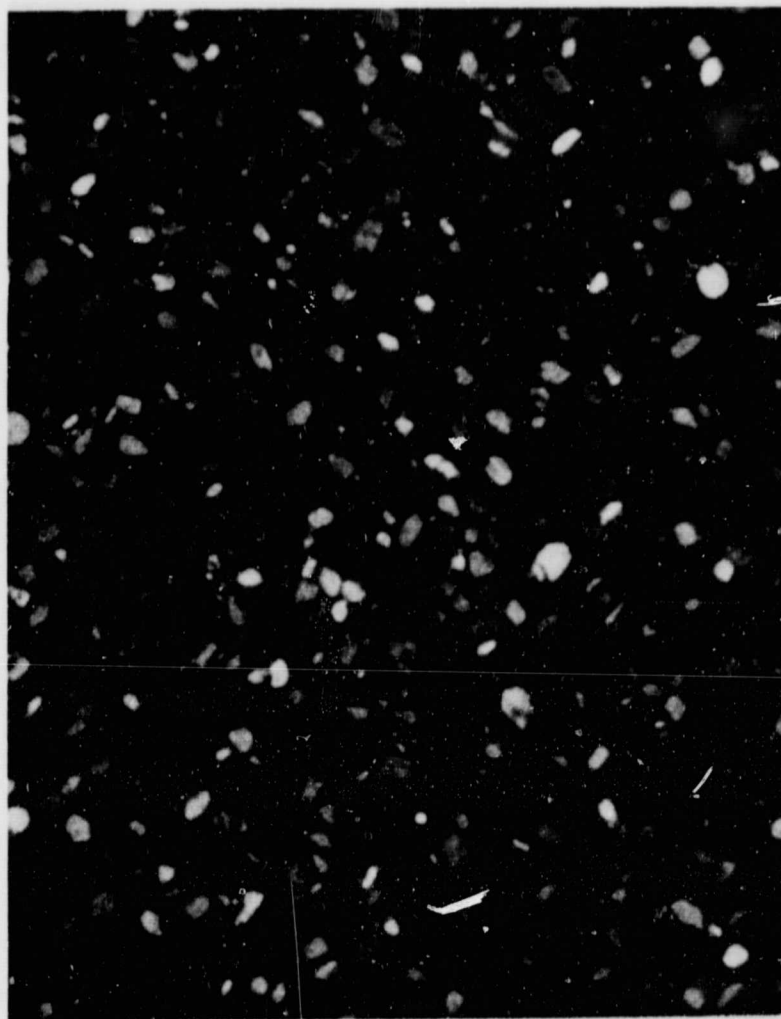


PHOTOMICROGRAPH OF SURFACE OF DEPOSITED CdS FILM



DEPOSITION SEQUENCE:  $\text{Cd Cl}_2 + \text{Cu} + \text{CdS}$   
(SLOW HEAT PROCESSING)

MAGNIFICATION 940 X



DEPOSITION SEQUENCE:  $\text{Cd Cl}_2 + \text{Cu} + \text{CdS}$   
(SLOW HEAT PROCESSING)

MAGNIFICATION 940 X

oriented with the C-axis oriented at an angle but definitely not parallel to the substrate.

- (4) The results of the emission spectrography are indicated below:

Element	Weight % in CdS
Cd	Matrix
In	Not detected
Cu	Trace
Fe	Trace
Mg	Trace
Cr	Trace

From the above tests it has been concluded that mechanical defects are introduced into the film depending upon the stage at which  $\text{CdCl}_2$  is added to the CdS film and on the method of post heat treatment. CdS films are obtained free of mechanical defects when the  $\text{CdCl}_2$  is evaporated first onto the substrate, followed by a layer of Cu and CdS with a subsequent heat treatment which spans several minutes.

VII. CONCLUSIONS AND RECOMMENDATIONS

Based on the work performed to date in investigating a multi-element detector strip and thin film readout techniques and the results obtained, the following conclusions were reached:

Analysis indicates that star detection by integration can produce usable signal levels from the photon irradiance produced by typical stars.

A detector strip fabricated by thin film photoconductor/ferroelectric techniques is capable of integrating a series of light pulses with a linearity that is satisfactory for system use.

Thin film transistors that are implemented with the same CdS-Se material as used in the detector strip exhibit switching characteristics that should be adequate to provide readout and readin commutation.

As a next step, the experience and capability that has been gained should be applied to the design and fabrication of a pilot star detection system.

## Appendix I

### STAR DETECTOR CONCEPT

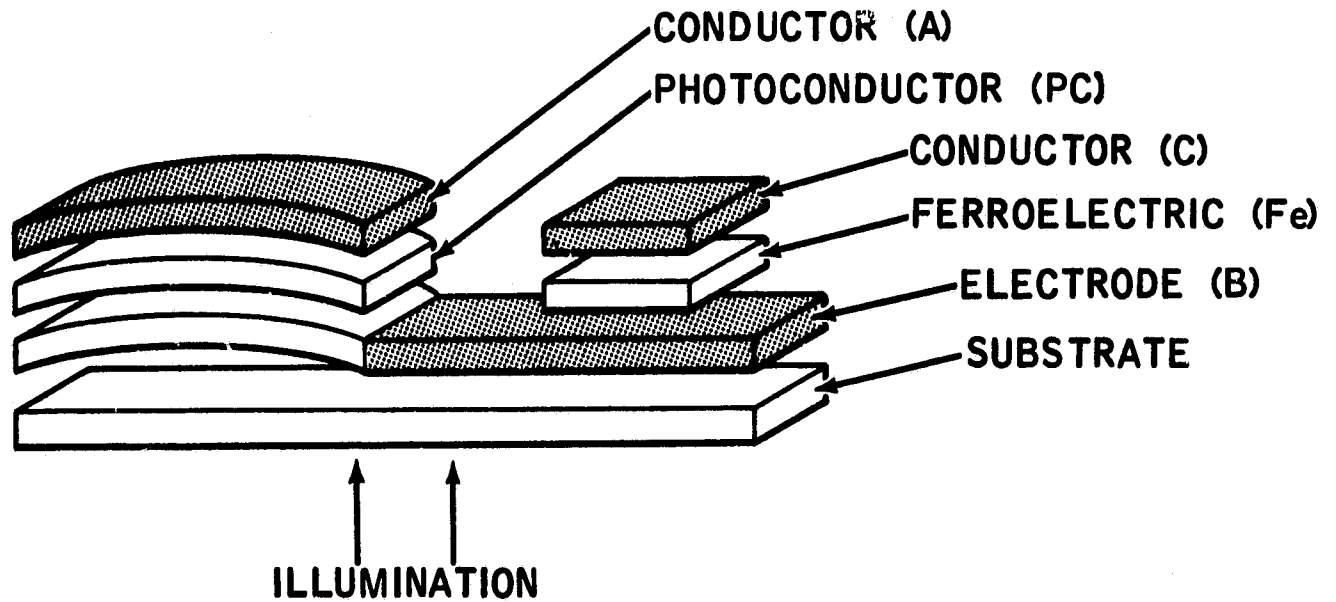
The star detector concept is based on a unique combination of a thin film photoconductor for optical sensing and a highly non-linear dielectric material, i.e., ferroelectric, for signal integration and storage. An elemental area of such a detector is shown in Figure 18 together with an equivalent electrical circuit. Essentially, during exposure, incident light flux from a radiant point source controls the current flowing through the photoconductor above its dark current value. The ferroelectric material, in turn, integrates and stores the signal by an internal polarization proportional to the charge. This internal polarization, unlike a linear dielectric material such as used in capacitors, is permanent until an equal charge of opposite polarity is applied for readout. The use of these two materials, therefore, permits the individual optimization of both of these functions.

Figure schematically depicts a multielement detector array and related optics. When the optics and detector array are made to rotate about the spin axis of a spin stabilized spacecraft, the detector progressively views an annular ring of the star field. For purposes of exposure, an electronic gating action is effected by the application of a "write" voltage. By gating the detector array at predetermined intervals of the vehicular spin, the same sector of the star field can be interrogated several times, or the whole star field can be sequentially scanned. The electronic gating, then, is equivalent to optically shuttering of the star image. The duration of the electronic shuttering signal determines the size of the sector of the annular field to be viewed, i.e., the angular field of view. The number of exposures of a given sector and the signal amplitudes determine the magnitude of charge stored in a given area of the ferroelectric. Signal integration by this method greatly increases the sensitivity of the system, permitting much weaker stars to be sensed or much smaller optical apertures to be used than normally possible with a single short exposure.

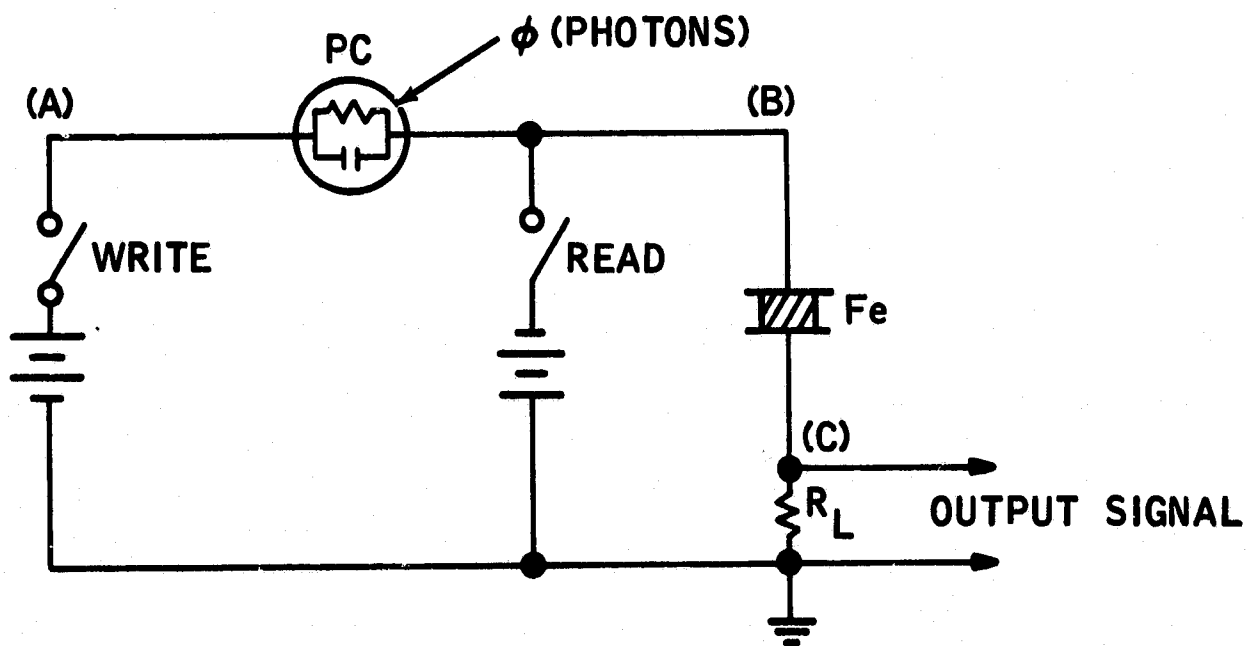
In operation, once having acquired the star signals as stored charge in the ferroelectric by electronically shuttering and integrating the incoming signals, data is sequentially readout from each ferroelectric element by means of a readout voltage of opposite polarity to the write voltage. The resultant current flowing through the output or load resistor and its time duration are a function of stored charge and represent the output signal. This reverse current flow discharges the ferroelectric resulting in a reversal of the internal polarization and preparing the ferroelectric for the next exposure.

## DETECTOR ELEMENT

### A. LAMINATE

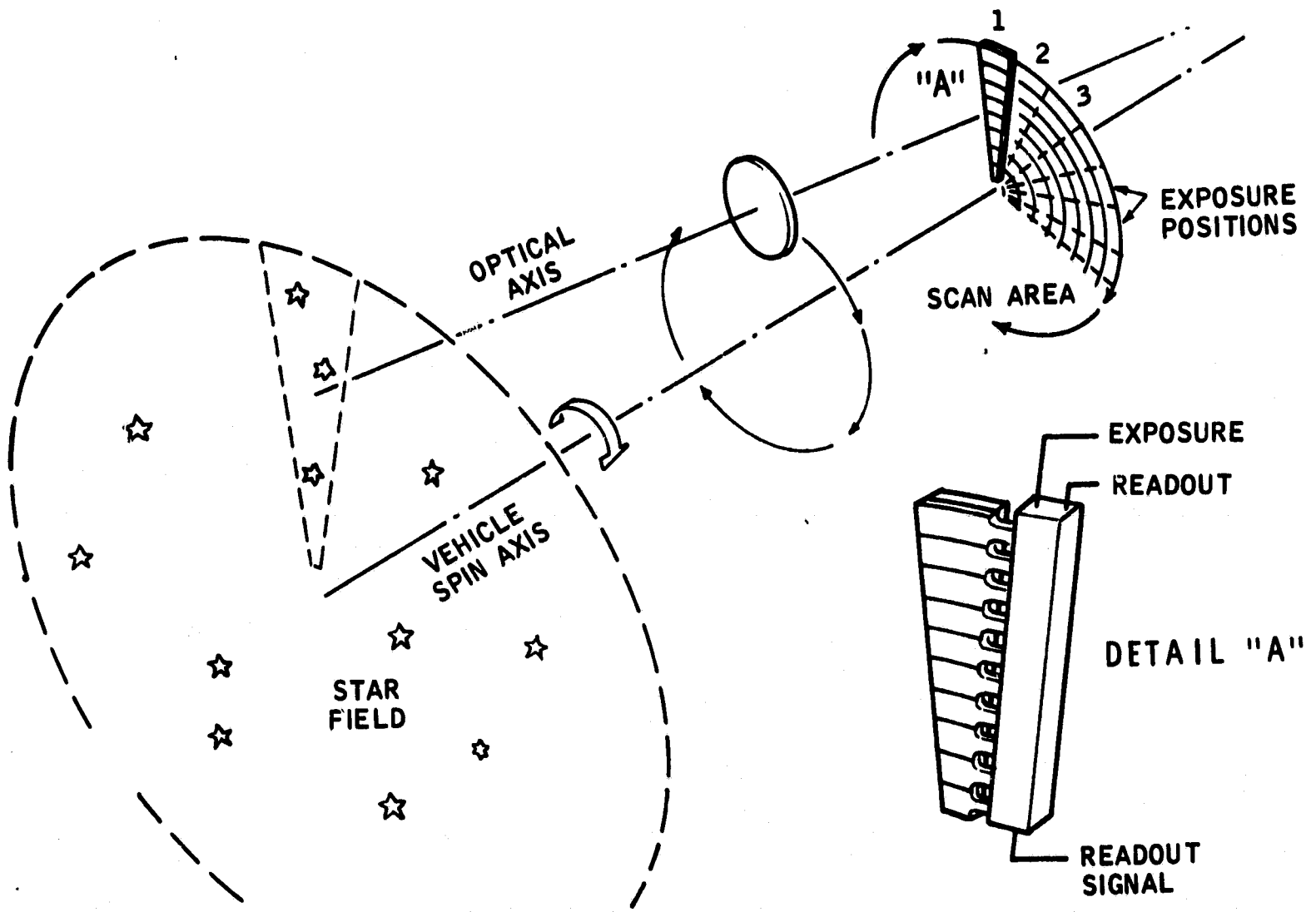


### B. EQUIVALENT CIRCUIT



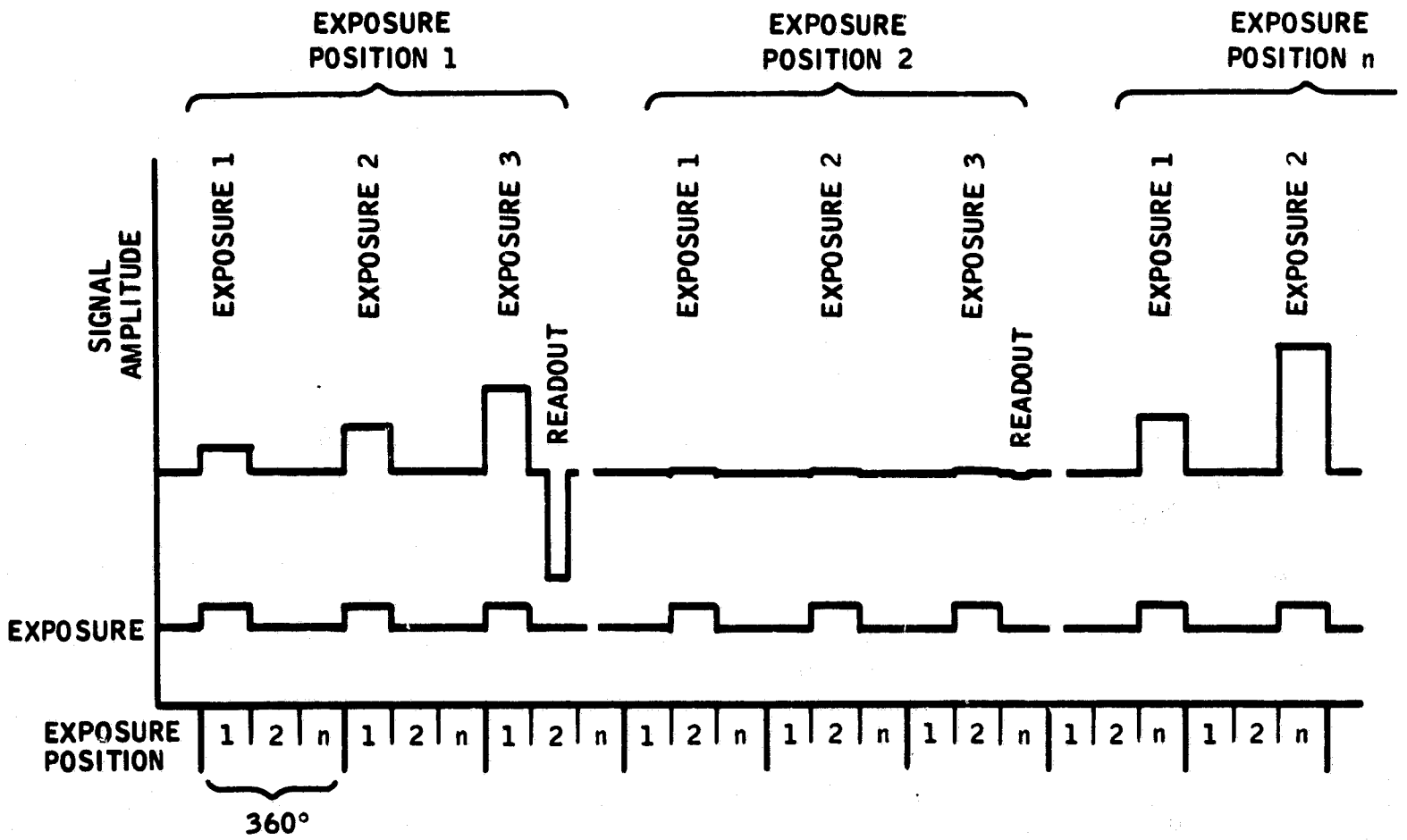


# MULTIELEMENT DETECTOR FOR STAR PATTERN RECOGNITION SYSTEM



The previous state of ferroelectric polarization is a function of the exposure value. For very weak optical signals and/or very short exposures, several exposures (light integration capability) may be required to charge the ferroelectric to its full value of internal polarization. Figure 20 depicts the signal acquired by one element during several spin revolutions of a spacecraft prior to reading the stored charge. In effect, variable brightness sources or a gray scale image can be sensed and read which is indicative of image photon magnitude. Figure 20 shows graphically the partial polarization as a function of light intensity and photoconductor current. As shown, the photoconductor current as a function of amplitude of incident light has a superlinear region between threshold and saturated current levels.

## MULTIPLE EXPOSURE FOR LOW LIGHT LEVEL INTEGRATION SINGLE ELEMENT



## Appendix II

### STAR BRIGHTNESS COMPUTATION

To fully evaluate the system parameters in a star detection system, it is necessary to define relative star brightness with respect to a given photosensor. This brightness can be defined by a rating system which takes into account the fact that all commonly used photosensitive devices do not have spectral response characteristics similar to the human visual response.

Magnitude scales are generally used to indicate the radiation from a star and the most common scale is the visual or photovisual scale. In this scale, the gradient between successive magnitudes is such that the lower magnitude in sequence is the fifth root of 100 or 2.512 times lighter than the star of immediately higher order magnitude.

The visual magnitude of a star is its relative intensity to the human eye by the conventional relationship:

$$\frac{I_1}{I_2} = (2.512)^{M_{v2} - M_{v1}} \quad (1)$$

Where  $I_1$  and  $I_2$  are the intensities of stars 1 and 2, and  $M_{v2}$ ,  $M_{v1}$ , their respective magnitudes in the visual scale.

The refinement brought to the Ptolemy scale, which has been accepted, was in the definition of the zero magnitude, which defines such illumination as  $2.1 \times 10^{-10}$  lumen  $\text{cm}^{-2}$  or,  $3.1 \times 10^{-13}$  watt  $\text{cm}^{-2}$ .

$$E_0 = \frac{2.1 \times 10^{-10}}{(2.512)^{M_v}} \text{ lumen cm}^{-2} \quad (2)$$

Other star magnitude scales are applicable whenever another detector is substituted for the human eye, such as photographic films and electrical detectors. However, by convention, all magnitude scales are normalized to give the same magnitude for an A0 star.

Since stars display variation in color, radiometric magnitude scales are useful for comparing detectors having different spectral responses. The radiometric scale is based on the equivalent black body temperature; it gives the total radiation received through one air mass, at the zenith.

The radiometric magnitude of many stars is given by the Draper classification, or by Pettit and Nicholson from data taken at Mount Wilson. These values can be easily corrected for outside atmosphere or sea level readings. The use of Mount Wilson data (5,000 feet) is a satisfactory approach for most star tracking applications and avoids inaccuracies in applying atmospheric corrections.

The total irradiance expressed as a function of the radiometric magnitude  $M_r$ , takes the same form as (2):

$$H_o = \frac{1.2 \times 10^{-12}}{(2.512)^{M_r}} \text{ watts cm}^{-2} \quad (3)$$

Thus, the radiation in the spectral region of interest can be calculated from Planck's law, if the stars are assumed to radiate as black bodies. Experimental results on a number of stars do not indicate significant deviations. The primary deviation from Planckian characteristics are due to absorption lines from the star atmosphere and to earth atmospheric absorption. This is evidenced by Balmer's discontinuity, which cuts off the continuum radiation below 3650 Angstroms, and the high intensity emission exhibited by the outer stellar atmosphere. However, neither of these restrictions is important if the response of the detector is confined to the 0.4 to 1 micron region.

Each spectral type of star has been assigned an effective color temperature. These assigned values are based on data from color index, heat index, energy and star diameter measurements. The Draper catalog, also known as Harvard's classification, contains several hundred thousands of referenced stars.

The color index of a star is the difference between its magnitude determined in two distinct colors, i.e., with  $M_B$  given in blue light:

$$M_B - M_V = \text{Color index}$$

The heat index follows from application of Wien's law, and is given as:

$$M_V - M_r = \text{Heat index}$$

with  $M_r$ , the radiometric magnitude.

Quantum detectors such as silicon, gallium arsenide, cadmium sulfide, etc., respond to the number of incident photons rather than to the incident energy. It is more convenient to use a photon magnitude scale rather than an energy scale in the evaluation of such quantum detectors for star tracker applications.

Such a photon magnitude scale is derived from power and wavelength, i.e., from the radiometric scale and the temperature of a star. As mentioned before, this new magnitude must be equal to the radiometric magnitude for an A0 star.

Hence, the ratio of photons rate to watts for an 11,000 °K black body is from Stephan's law:

$$\lambda_0 = \frac{2.896}{11 \times 10^3} = 0.263 \text{ micron}$$

and

$$\frac{P}{P_0} = \frac{10^7}{0.263 \times 1.6 \times 10^{-12}}$$

$$= 2.45 \times 10^{18} \text{ photon sec}^{-1} \text{ watt}^{-1} \quad (4)$$

Combining (3) and (4) gives the photon irradiance for a zero magnitude A0 star:

$$\phi_0 = \frac{PH}{P_0} = 2.45 \times 10^{18} \times 1.2 \times 10^{-12}$$

$$= 2.94 \times 10^6 \text{ photon sec}^{-1} \text{ cm}^{-2} \quad (5)$$

Therefore, the new magnitude relationship is given by

$$\phi = \frac{2.94 \times 10^6}{(2.512)^{M_p}} \text{ photon sec}^{-1} \text{ cm}^{-2} \quad (6)$$

where  $\phi$  is the photon irradiance from the star and  $M_p$  is the photon magnitude of the star.

We can now calculate the photon magnitude for the various star temperatures. This is accomplished by multiplying the star energy (3) by the ratio of photon per second to watts, for each temperature. Setting the product equal to the photon irradiance (6), and solving for the photon magnitude,

$$\frac{1.2 \times 10^{-12}}{(2.512)^{M_r}} \frac{\sigma_o T^3}{\sigma T^4} = \frac{2.94 \times 10^6}{(2.512)^{M_p}} \text{ photon sec}^{-1} \text{ cm}^{-2} \quad (7)$$

where  $\sigma = 5.67 \times 10^{-12} \text{ watt cm}^{-2} \text{ deg}^{-4}$  (Stephan's constant)  
 $T = \text{temperature in degrees Kelvin}$   
 $\sigma_o = 1.52 \times 10^{11} \text{ photon sec}^{-1} \text{ deg}^{-3}$  (Stephan-Boltzmann photon constant)

The constant,  $\sigma_o$ , results from the integration from 0 to for the total number of photons in the zone of the spectrum of the black body. The expression for total photons corresponds to the Stephan-Boltzmann equation for total radiation but the total emission of photons varies as  $T^3$  not as  $T^4$ .

The difference between photon and radiometric magnitude is plotted in Figure 21, for a limited range of temperature corresponding approximately to the extreme magnitudes taken in the following examples.

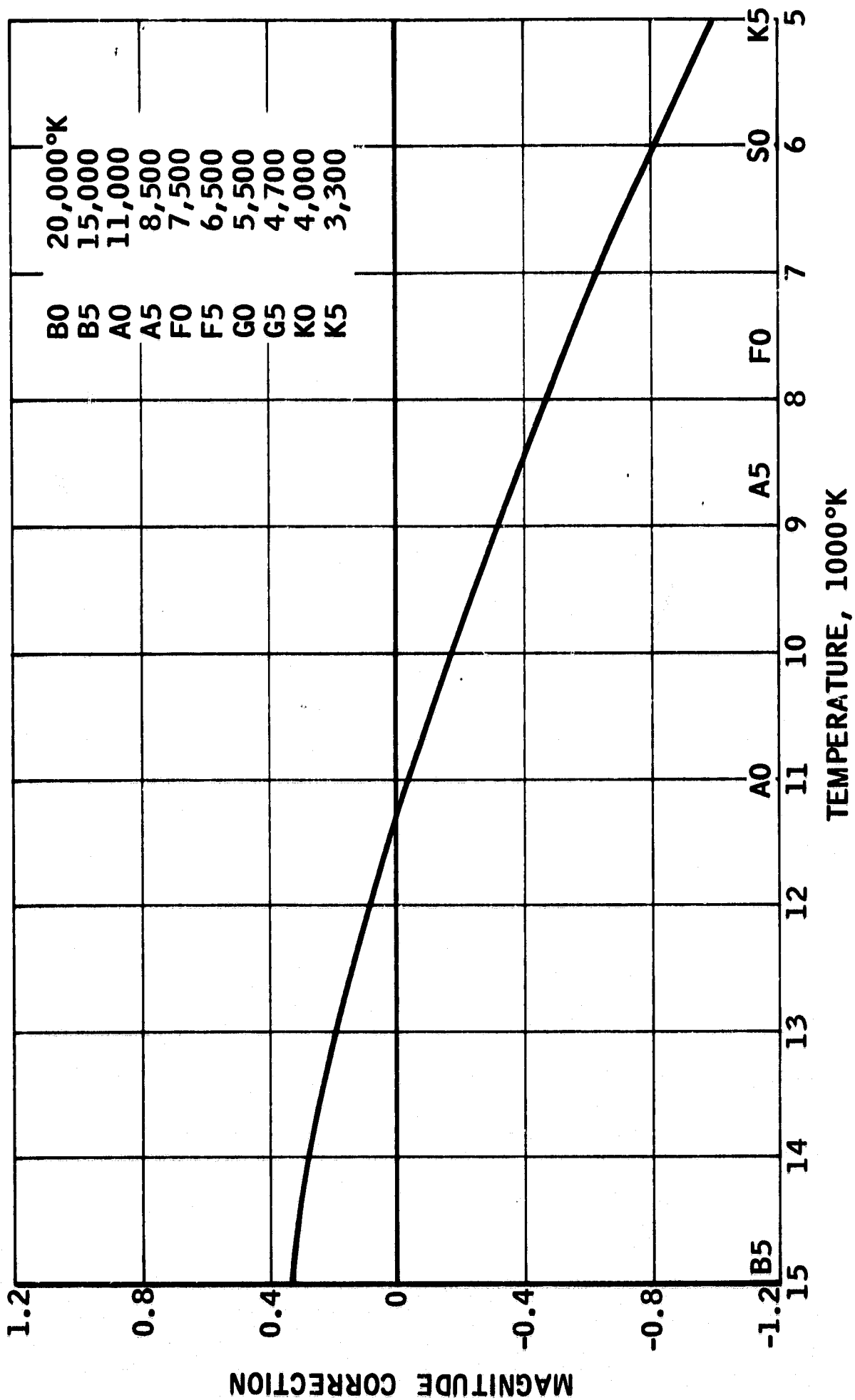
To calculate the photon irradiance in a given spectral region, the total photon irradiance  $\phi$  from (6) is multiplied by the photon percentage that falls in the wavelength interval described by the spectral range:

$$\phi_{\Delta\lambda} = \frac{2.94 \times 10^6}{(2.512)^{M_p}} \frac{\int_{\lambda_1}^{\lambda_2} c_1 \lambda^{-4} \left(\exp \frac{c_2}{\lambda T} - 1\right) d\lambda}{\sigma_o T^3} \quad (8)$$

where the constant,  $c_1 = 1.88 \times 10^{11} \text{ sec}^{-1} \text{ cm}$

$c_2 = 1.438 \text{ cm}^\circ\text{K}$

CORRECTION FROM RADIOMETRIC TO PHOTON MAGNITUDE





If a narrow spectral band is used to evaluate the performance of the detector, equation (8) may be simplified for star radiation calculation by using the percentage of power in a narrow spectral band, which gives

$$\%W = \frac{W \Delta \lambda}{W_{\text{total}}} = \frac{2 \pi h c^2 \Delta \lambda}{\lambda^5 \left( \exp \frac{ch}{\lambda kT} - 1 \right) \sigma T^4} \quad (9)$$

Therefore, the irradiance, H, in the narrow spectrum range is the product of (3) and (9)

$$H = \frac{7.9 \times 10^{-18} \Delta \lambda}{\lambda^5 T^4 (2.512)^{M_r} \exp\left(\frac{1.436}{\lambda T}\right) - 1} \text{ watt cm}^{-2} \quad (10)$$

and similarly, evaluating the photon irradiance,

$$\phi = \frac{4 \times 10^{10} \Delta \lambda}{\lambda^4 T^4 (2.512)^{M_r} \exp\left(\frac{1.436}{\lambda T}\right) - 1} \text{ photon sec}^{-1} \text{ cm}^{-2} \quad (11)$$

Selecting stars as practical examples of computation

**Alpheratz** the  $\alpha$  star in the constellation of Andromeda, which from (7) gives a photon magnitude,  $M_p$ , of 2.1

**Hamal** the  $\alpha$  star in the constellation of Aries, which from (7) gives a photon magnitude of 0.06

Computing from (8), the photon irradiance from these two stars, two spectral ranges of detection can be assigned which fit the two extreme types of detectors, i.e., silicon-A and cadmium sulfide - B,

**Alpheratz** AO star; 11,000<sup>0</sup> K;  $M_r$  2.2;  $M_p$  2.1

$$\Delta \lambda = 0.5 \text{ to } 1 \text{ micron } \phi = \frac{2.44 \times 10^6}{(2.512)^{2.1}} \times 0.357 = 1.5 \times 10^5 \text{ photons sec}^{-1} \text{ cm}^{-2}$$

$$B \Delta \lambda = 0.5 \text{ to } 0.7 \text{ micron } \phi = \frac{2.44 \times 10^6}{(2.512)^{2.1}} \times 0.185 = 7.8 \times 10^4 \text{ photons} \\ \text{sec}^{-1} \text{ cm}^{-2}$$

Hamal K2 star; 3780°K;  $M_r$  2;  $M_p$  0.06

$$A \Delta \lambda = 0.5 \text{ to } 1 \text{ micron } \phi = \frac{2.44 \times 10^6}{(2.512)^{0.06}} \times 0.234 = 6.5 \times 10^5 \text{ photons} \\ \text{sec}^{-1} \text{ cm}^{-2}$$

$$B \Delta \lambda = 0.5 \text{ to } 0.7 \text{ micron } \phi = \frac{2.44 \times 10^6}{(2.512)^{0.06}} = 1.7 \times 10^5 \text{ photons} \\ \text{sec}^{-1} \text{ cm}^{-2}$$